THEORY AND APPLICATION OF THE POTENTIAL STEP-LINEAR SCAN ELECTROLYSIS METHOD.

KINETICS AND MECHANISM OF REDUCTION OF SUBSTITUTED AZOBENZENE COMPOUNDS

Thesis for the Degree of Ph. D.
MICHIGAN STATE UNIVERSITY
Joseph Theodore Lundquist, Jr.
1967



## This is to certify that the

## thesis entitled

THEORY AND APPLICATION OF THE
POTENTIAL STEP-LINEAR SCAN
ELECTROLYSIS METHOD.
KINETICS AND MECHANISM OF
REDUCTION OF SUBSTITUTED AZOBENZENE COMPOUNDS

Joseph Theodore Lundquist, Jr.

has been accepted towards fulfillment of the requirements for

Ph.D. degree in \_\_\_\_\_

Reduced Trich Ga.

Major professor

Date November 27, 1967

#### ABSTRACT

THEORY AND APPLICATION OF THE POTENTIAL STEP-LINEAR
SCAN ELECTROLYSIS METHOD.
KINETICS AND MECHANISM OF REDUCTION OF
SUBSTITUTED AZOBENZENE COMPOUNDS

by Joseph Theodore Lundquist, Jr.

Theory for the potential step-linear scan technique for the case of a chemical reaction following reversible electron transfer has been developed without the use of simplifying approximations introduced by previous authors. Results of the theoretical calculations are presented in the form of working curves from which homogeneous kinetic parameters are easily determined. Results of the theory indicate that this technique should be a versatile method for studying electrode processes and measuring homogeneous rate constants. These conclusions are illustrated by measuring rates of benzidine rearrangement of hydrazobenzene and m-hydrazotoluene. In the case of the latter compound a direct comparison is given between rate constants measured electrochemically and by classical kinetic methods, and it is concluded that homogeneous rate constants can be measured electrochemically with complete confidence.

The mechanism of the electrode reaction for reduction of azobenzene also has been investigated in detail in aqueous and non-aqueous solvents. Because of the unambiguous mechanism found in N,N-dimethylformamide several substituted azobenzene compounds were studied in an attempt to correlate

reactivity with structure. Both half-wave potentials and standard heterogeneous rate constants gave linear correlations with Hammett  $\underline{\sigma}$  values.

To explain results obtained in aqueous solutions a general mechanism was proposed where hydrogen ions participate in preceding and succeeding chemical equilibria and also in the rate determining step of the electrode reaction. Theory of cyclic voltammetry was extended to include this general mechanism. Experimental results for reduction of azobenzene were found to be consistent with two electrons and two hydrogen ions involved in the rate determining step. However, additional experimental data that suggest stepwise reduction, which also would be consistent with the cyclic voltammetric data, are presented.

# THEORY AND APPLICATION OF THE POTENTIAL STEP-LINEAR SCAN ELECTROLYSIS METHOD.

# KINETICS AND MECHANISM OF REDUCTION OF SUBSTITUTED AZOBENZENE COMPOUNDS

Ву

Joseph Theodore Lundquist, Jr.

## A THESIS

Submitted to
Michigan State University
in partial fulfillment of the requirements
for the degree of

DOCTOR OF PHILOSOPHY

Department of Chemistry

1967

650143

## VITA

NAME: Joseph Theodore Lundquist, Jr.

BORN: May 2, 1940 in Bay City, Michigan

## ACADEMIC CAREER:

Midland High School Midland, Michigan (1954-1958)

Michigan State University East Lansing, Michigan (1958-1967)

## DEGREES HELD:

B.S. Michigan State University (1963)

M.S. Michigan State University (1965)

### ACKNOWLEDGMENTS

The author wishes to express his appreciation to Dr. Richard S. Nicholson for his guidance and encouragement throughout this study.

The author is grateful to the Socony Mobil Oil Company,
United States Army Research Office--Durham under Contract
No. DA-31-124-ARO-D-308, and the Department of Chemistry
for financial aid.

Special thanks go to the author's wife, Joann, for assistance rendered throughout the course of his graduate studies.

## TABLE OF CONTENTS

	Page
INTRODUCTION	. 1
DESCRIPTION OF POTENTIAL STEP-LINEAR SCAN TECHNIQUE	. 3
THEORY	. 9
Solution of the Integral Equation	. 14
Results of Numerical Calculations	17
Measurement of Rate Constants	. 26
EXPERIMENTAL EVALUATION OF POTENTIAL STEP-LINEAR	
SCAN THEORY	30
EXPERIMENTAL	33
Instrumentation	. 33
Chemicals	43
Procedures	43
RESULTS AND DISCUSSION	45
Effects of Gelatin	45
Reduction of Azobenzene	58
Reduction of m-Azotoluene	65
Comparison of Rate Constants	69
REDUCTION OF AZOBENZENE IN N,N-DIMETHYLFORMAMIDE .	. 71
EXPERIMENTAL	. 74
Materials	. 74
Solvent	74
Chemicals	74
Procedures	. 75
Solutions	. 75
Evaluation of Diffusion Coefficients	. 77
Evaluation of $\underline{\mathbf{E}_1}/_2$	. 77
Measurement of Heterogeneous Rate Constant	s 77
RESULTS AND DISCUSSION	. 80
Evaluation of Diffusion Coefficients	. 84
Comparison of Measured Diffusion Coef-	_
ficients with Stokes-Einstein Diffusion	
Theory	. 84
Effect of Double Layer Structure on	
Heterogeneous Rate Constants	. 88

# TABLE OF CONTENTS (Cont.)

	Page
Applicability of the Hammett Equation Variation of Half-Wave Potentials with	90
Structure	94
with Structure	95
MECHANISM OF REDUCTION OF AZOBENZENE IN WATER	100
THEORY	101
EXPERIMENTAL	105
RESULTS AND DISCUSSION	106
LITERATURE CITED	122
APPENDIX A	126
APPENDIX B	128

## LIST OF TABLES

TABLE	I	age
ı.	Variation of $\sqrt{\pi} \chi_p$ with $\underline{k}/\underline{a}$ and $\underline{a\lambda}$	28
II.	Polarographic data for the reduction of azobenzene at various gelatin and acid concentrations	47
III.	Comparison of rate constants for rearrangement of hydrazobenzene determined with and without gelatin present	51
IV.	Diffusion coefficients of azobenzene for different acid and gelatin concentrations .	55
٧.	Rate constants for rearrangement of $\underline{m}$ -hydrazotoluene	66
VI.	Comparison of observed and literature values for melting points of substituted azobenzene compounds	76
VII.	Diffusion coefficients of substituted azobenzene compounds in N,N-dimethylformamide .	84
VIII.	$\frac{E_1}{i}$ and $\frac{k}{i}$ values for azobenzene compounds in N,N-dimethylformamide	92
IX.	Variation of $\underline{E_1}/2$ and $(\underline{k_s})_{app}$ with hydrogen ion concentration for reduction of azobenzene in aqueous solutions	107

## LIST OF FIGURES

Figure		Page
1.	(a) Applied potential as a function of time for potential step-linear scan method; (b) current-time curves for large and small rate constants	5
2.	Variation of current function with $\underline{k}/\underline{a}$ (0.1, 0.05, 0.01) for $\underline{a}\underline{\lambda}$ = 15	18
3.	Variation of anodic peak potential with $k/a$ for $a\lambda = 0.5$ and $62.5 \dots \dots \dots \dots$ .	21
4.	Variation of peak current function with $k/a$ for $\underline{a\lambda}$ = 0.5, 2.5, 7.5, 20.0, 37.5 and 62.5 .	24
5.	Circuit diagram of potentiostat with floating load resistor	34
6.	Circuit diagram of modified potentiostat	37
7.	Cell arrangement	40
8.	Conventional polarographic current-potential curves showing effects of gelatin on reduction of azobenzene	n 49
9.	Stationary electrode polarograms showing effects of gelatin on reduction of $\underline{mM}$ azobenzene (scan rate, 30 mv sec <sup>-1</sup> )	52
10.	Chronoamperometric curves showing effects of gelatin on reduction of azobenzene	56
11.	Comparison of theory and experiment for potential step-linear scan method	<b>-</b> 60
12.	Variation of $\underline{k}$ with $H_0$ for the benzidine rearrangement of hydrazobenzene	63
13.	Variation of $\underline{k}$ with concentration of perchloric acid for rearrangement of $\underline{m}$ -hydrazotoluene	67
14.	Cyclic stationary electrode polarogram for reduction of $\underline{mM}$ azobenzene in $0.3\underline{M}$ tetraethylammonium perchlorate and N,N-dimethylformamide (scan rate, $40 \text{ v sec}^{-1}$ )	81

## LIST OF FIGURES (Cont.)

Figure		Page
15.	Variation of diffusion coefficient of substituted azobenzene compounds with molecular weight (error level, $\pm 0.2 \times 10^{-6}$ cm <sup>2</sup> sec <sup>-1</sup> )	86
16.	Variation of $\underline{E_1}/_2$ with Hammett $\underline{\sigma}$ value for substituted azobenzene compounds (slope, 0.36 volts; $\underline{E_1}/_2$ $\underline{vs}$ S.C.E.)	93
17.	Variation of $\underline{k}$ with Hammett $\underline{\sigma}$ value for substituted azobenzene compounds (slope, 0.43 $\pm$ 0.03; error level, $\pm$ 10%)	97
18.	Variation of $\underline{\mathbf{E}}_1'$ with perchloric acid concentration for reduction of azobenzene (slope, 56 mv per unit pH change; $\underline{\mathbf{E}}_1/_2$ vs S.C.E.).	108
19.	Variation of $\left(\frac{k}{s}\right)_{app}$ with perchloric acid concentration for reduction of azobenzene (slope, 0.76)	110
20.	Variation of $(\underline{k}_s)_{app}$ with $[H^+]^{0.76}$ for reduction of azobenzene (slope, 0.105 cm sec <sup>-1</sup> )	112
21.	Comparison of theory and experiment	115
22.	Cyclic stationary electrode polarograms for reduction of $0.4  \underline{\text{mM}}$ azobenzene in $0.3\underline{\text{M}}$ tetraethylammonium perchlorate and N,N-dimethylformamide with varying amounts of benzoic acid (scan rate, $40  \text{v}  \text{sec}^{-1}$ )	118

#### INTRODUCTION

Whenever a chemical reaction can be initiated electrolytically

$$\begin{array}{ccc}
0 + ne & \xrightarrow{\times} & R \\
R & \xrightarrow{k} & Z
\end{array}$$

electrochemical techniques possess some unique advantages over more classical approaches for studying kinetics of the chemical reaction. For example, because the reacting intermediate, R, is generated at the electrode, this same electrode can be used to follow the concentration of R, and as a result kinetics of very rapid chemical reactions can be measured. Although several electrochemical techniques have been developed for studies of this type, many of these techniques are limited for one reason or another. One method which appeared to have a minimum of limitations is the potential step-linear scan technique. Although this method seemed to be potentially very important, a quantitative development had not been reported, and therefore this task was adopted as the major goal of this thesis. Thus, the majority of the thesis is devoted to theoretical development and experimental applications of the potential step-linear scan method.

The experimental applications involve studies of benzidine rearrangements which are initiated by reduction of azobenzene. For purposes of evaluating the potential steplinear scan method these reductions were performed under conditions where the electrode reaction is reversible. Because of this no information about the actual mechanism of the electrode process was required, or obtainable for that matter. However, after establishing the usefulness of the potential step-linear-scan technique, it was logical to attempt heterogeneous kinetic studies of the electrode reaction in an effort to determine its mechanism. To do this it also was necessary to determine the role of hydrogen ion, and therefore experiments were performed in an aprotic solvent as well as in water. Results of these mechanistic studies also are included in this thesis.

### DESCRIPTION OF POTENTIAL STEP-LINEAR SCAN TECHNIQUE

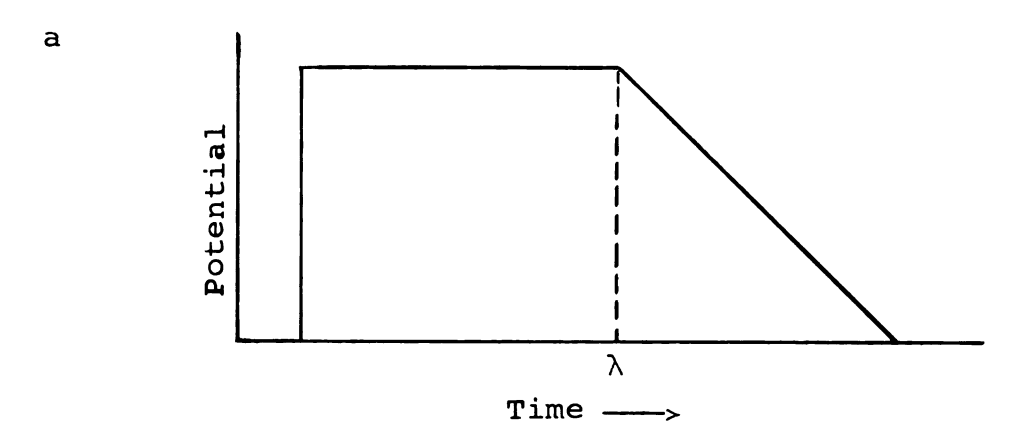
Several different electrochemical techniques are suitable for investigation of Mechanism I. These methods differ primarily in the form of the external perturbation applied to the electrode, and can be classified as either one-step or two-step methods. The one-step techniques are exemplified by conventional polarography (1-4) where removal of R from the electrochemical equilibrium results in a shift of  $\mathbb{E}_{1/2}$  and distortion of the current-voltage curve from that expected for reversible uncomplicated reduction. The magnitude of these effects is related to the rate constant,  $\underline{\mathbf{k}}$ . These indirect methods are of limited use, however, because the above parameters are relatively insensitive to changes of  $\underline{\mathbf{k}}$ , and also  $\underline{\mathbf{E}}_{1/2}$  in the absence of kinetic complications must be known.

With the two-step methods R is generated at a controlled rate during the first step, and then unreacted R is measured in the second step. The change in the amount of R observed relative to the case with no kinetic complications gives a measure of  $\underline{k}$ . These two-step techniques have the advantage that it is unnecessary to know  $\underline{E_1}/_2$  in the absence of kinetic complications. Typical of these methods are chronopotentiometry with current reversal (5-8), controlled potential step-functional electrolysis (9), and cyclic voltammetry (10). A fourth technique, the potential step-linear scan method, is a combination of the last two methods—i.e., a voltage

step is applied to the electrode, followed by a linear potential scan (Figure 1a).

To explain qualitatively the effect of Mechanism I on a potential step-linear scan experiment, it is useful to consider the two parts of the experiment separately. The first part (t  $\leq \lambda$ , see Figure 1) consists of a controlled potential generation of the intermediate, R. The second part  $(t > \lambda)$  is the measurement step in which stationary electrode polarography is used to analyze for unreacted R. During the generation step the current will follow normal diffusion controlled decay, provided potential is stepped to a value corresponding to the limiting current region (Figure 1b). Current during this part of the experiment is unaffected by the chemical reaction, because at limiting current potentials, current is determined only by the rate of arrival of substance O at the electrode surface. However, during the measurement step currents should be markedly affected by the chemical reaction. Consider, for example the case where the chemical reaction is slow (or, equivalently, scan rate is relatively large). The current for this case should be large, because essentially all of R remains in the vicinity of the electrode (see Figure 1b). As the rate of the chemical reaction increases, however, the resulting current should decrease because of the decrease of R near the electrode. By comparing this decrease of current with the diffusion controlled current  $(\underline{t} < \underline{\lambda})$ , it should be possible to determine the rate constant, k.

Figure 1. (a) Applied potential as a function of time for potential step-linear scan method; (b) current-time curves for large and small rate constants.



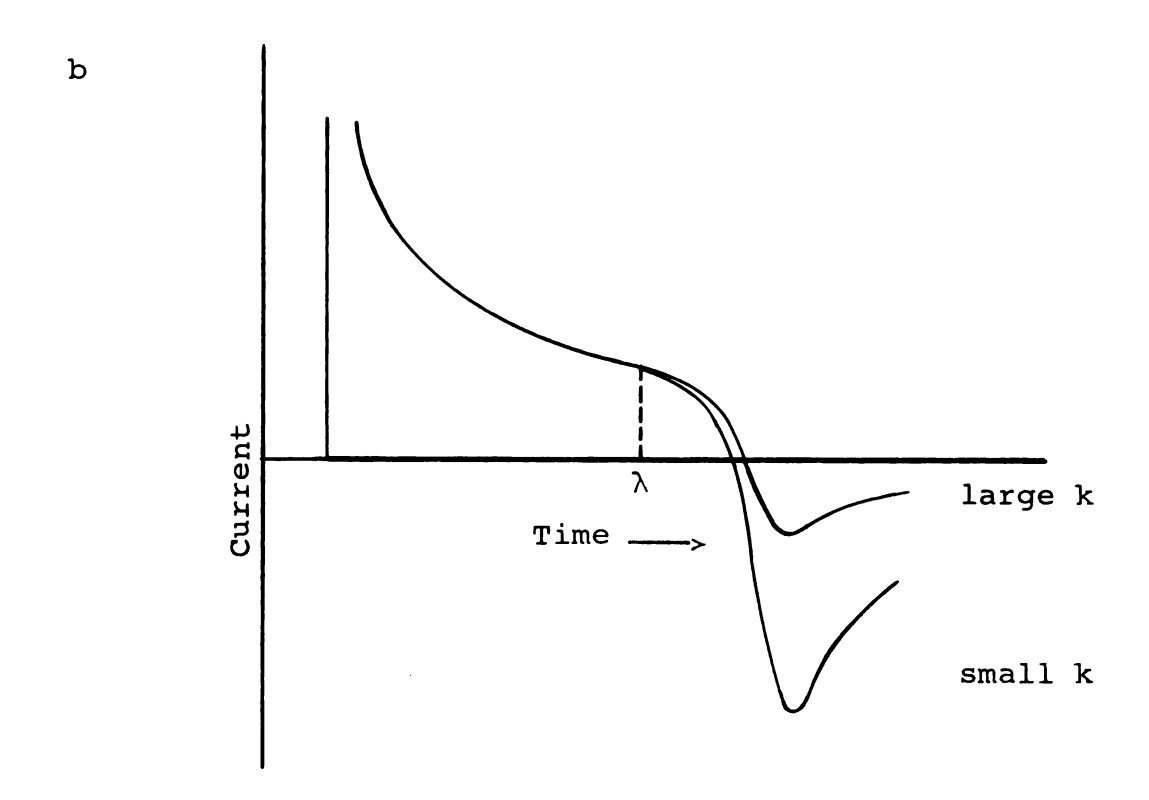


Figure 1

Based on the above discussion apparently the potential step-linear scan technique should possess some unique advantages over other electrochemical methods. For example, some of the best features of both square-wave electrolysis and cyclic voltammetry are combined. The method has the important advantage of square-wave electrolysis that adsorption effects are minimized because reduction of adsorbed material occurs only during the initial fraction of the experiment (9). The method has the additional advantage of cyclic voltammetry that the potential dependence of oxidation of R is retained as an experimental parameter. This potential dependence provides important information about the activated product, R, similar to polarographic half-wave potential data, but on a much broader time scale (10).

Because of the unique features of the potential steplinear scan technique, and its potentially important application in electrochemical studies, it seemed important to
attempt a rigorous theoretical development of the method.

During the course of this work, a theoretical treatment was
presented by Schwarz and Shain (11). The theory of these
authors, however, is inexact, and because of simplifying
approximations, application of their results is limited to
cases in which duration of the linear scan is small with respect to the half-life of the chemical reaction (11). This
means that scan rates must be used which are as much as two
orders of magnitude larger than actually necessary to detect
kinetic effects. Consequently, factors such as charging

current and charge transfer kinetics rapidly become limiting. In addition, it always is necessary to measure small changes of large peak currents, and considerable sensitivity is lost. For these reasons the theory of Schwarz and Shain is of limited usefulness compared with the rigorous treatment presented here.

#### THEORY

Development of a mathematical description of the potential step-linear scan method for Mechanism I is equivalent to calculating the concentration profiles of substances O and R. These concentration profiles depend on the potential perturbation employed (potential step-linear scan), and the mass transport process. Of the various types of mass transport, diffusion is the simplest to describe mathematically. Fortunately, by employing conventional polarographic conditions, it is possible to limit experimentally the mass transport process to diffusion, and therefore Fick's diffusion equations can be used to calculate concentrations of O and R (12,13). The diffusion equation for R, of course, must be modified to account for homogeneous kinetic reaction of R (10).

Application to substances O and R of Fick's second law for linear diffusion gives

$$\frac{\partial c_{O}(x,t)}{\partial t} = D_{O} \frac{\partial^{2} c_{O}(x,t)}{\partial x^{2}}$$
 (1)

$$\frac{\partial c_R(x,t)}{\partial t} = D_R \frac{\partial^2 c_R(x,t)}{\partial x^2} - k c_R(x,t)$$
 (2)

where  $C_O(x,t)$  and  $C_R(x,t)$  are concentrations of 0 and R respectively,  $\underline{x}$  is distance from the electrode surface,  $\underline{t}$  is time,  $D_O$  and  $D_R$  are diffusion coefficients, and  $\underline{k}$  is the first order rate constant for the homogeneous chemical reaction.

Solutions of Equations 1 and 2 contain integration constants which must be evaluated. To determine these constants initial and boundary conditions, which are mathematical statements of experimental conditions, must be formulated.

Initially concentrations of O and R are assumed to be equal to their bulk analytical values

$$t = 0; x \ge 0;$$
 $C_{O}(x,c) = C_{O}^{*}; C_{R}(x,c) = C_{R}^{*}(\sim 0)$  (3)

After the experiment is started it is assumed that a point sufficiently removed from the electrode surface exists beyond which there are no concentration gradients. This condition is readily satisfied, even for cells of small dimension (12). Mathematically this condition is

$$t > 0 ; x \longrightarrow \infty :$$

$$c_{O}(x,t) \longrightarrow c_{O}^{*} ; c_{R}(x,t) \longrightarrow c_{R}^{*}$$
(4)

A material balance equating rates of arrival of  $\,$ O and departure of  $\,$ R from the electrode surface provides the third boundary condition

$$t > 0 ; x = 0$$
:

$$D_{O}\left(\frac{\partial C_{O}(x,t)}{\partial x}\right) = -D_{R}\left(\frac{\partial C_{R}(x,t)}{\partial x}\right)$$
 (5)

To obtain the final boundary condition it will be assumed that the redox couple obeys the Nernst equation. To assume a more general potential-concentration relationship

would complicate the theory considerably (10,14). Moreover, it usually is possible to adjust conditions experimentally so that this assumption is satisfied. Thus, applying the Nernst equation to the redox couple, one obtains

$$x = 0 ; t \ge 0$$
:

$$\frac{C_O(o,t)}{C_R(o,t)} = \exp \left[ \left( \frac{nF}{RT} \right) \left( E - E^0 \right) \right]$$
 (6)

where  $\underline{n}$  is the number of electrons,  $\underline{E}$  is electrode potential,  $\underline{E^0}$  is the formal electrode potential, and R, T and F have their usual meaning.

For the potential step-linear scan technique Equation 6 is rewritten to account for variation of electrode potential with time (Figure 1a). The result of these operations is Equation 7

$$(nF/RT)(E_{i} - E^{0})$$
 t = 0 (7a)

$$ln(S_{\lambda}(at)) = (nF/RT)(E_{i} - E^{0} - E_{S})$$
  $0 < t \le \lambda$  (7b)

$$(nF/RT)(E_i - E^0 - E_S) + at - a\lambda t > \lambda$$
 (7c)

where

$$s_{\lambda}(at) = c_{0}(c,t)/c_{R}(o,t)$$
 (7d)

There  $\underline{\mathbf{E}}_{\mathbf{i}}$  is initial potential,  $\underline{\mathbf{E}}_{\mathbf{S}}$  is the potential to which the electrode is stepped,  $\underline{\lambda}$  is time at which linear scan begins (Figure 1a), and  $\underline{\mathbf{a}}$  is a parameter directly proportional to the scan rate,  $\underline{\mathbf{v}}$ , during the linear scan.

$$a = \frac{nFv}{RT} \tag{8}$$

To obtain general solutions of the above boundary value problem, it is useful first to reduce it to integral equation form (10). This reduction can be accomplished with the aid of the Laplace transformation (10). Hence Laplace transformation of Equations 1 to 3 yields

$$D_O \frac{\partial^2 C_O(x,s)}{\partial x^2} = s C_O(x,s) - C_O^*$$
 (9)

$$D_{R} \frac{\partial^{2}C_{R}(x,s)}{\partial x^{2}} = (s - k) C_{R}(x,s)$$
 (10)

where  $C(\underline{x},\underline{s})$  is the Laplace transform of  $C(\underline{x},\underline{t})$ . Equations 9 and 10 are ordinary differential equations, which, together with Equation 4, can be solved to give

$$C_O(x,s) = (C_O(0,s) - \frac{C_O^*}{s}) \exp [-x(\frac{s}{D_O})^{1/2}] + \frac{C_O^*}{s}$$
 (11)

$$C_{R}(x,s) = C_{R}(0,s) \exp \left[-x \left(\frac{s+k}{D_{R}}\right)^{1/2}\right]$$
 (12)

By differentiating Equations 1 and 12 with respect to  $\underline{x}$  and then evaluating at  $\underline{x} = 0$ , one obtains

$$D_{O}\left[\frac{\partial c_{O}(x,s)}{\partial x}\right]_{x=0} = -\left(c_{O}(0,s) - \frac{c_{O}^{*}}{\widehat{s}}\right)\sqrt{D_{O}s}$$
 (13)

$$D_{R} \left[ \frac{\partial C_{R}(x,s)}{\partial x} \right]_{x=0} = -C_{R}(0,s) \sqrt{D_{R}(s+k)}$$
 (14)

The left hand side of Equations 13 and 14 is the Laplace transform of the surface flux of 0 and R respectively.

Inversion of Equations 13 and 14 is accomplished with the convolution theorem of operational calculus (15).

Inversion followed by application of Equation 5 yields the following integral relationships between surface concentration and flux

$$c_{O}(o,t) = c_{O}^{*} - \frac{1}{\sqrt{\pi D_{O}}} \int_{0}^{t} \frac{f(\tau)d\tau}{\sqrt{t - \tau}}$$
 (15)

$$C_{R}(0,t) = \frac{\gamma}{\sqrt{\pi D_{O}}} \int_{0}^{t} \frac{f(\tau) \exp\{-k(t - \tau)\} d\tau}{\sqrt{t - \tau}}$$
 (16)

where

$$\gamma = \sqrt{\frac{D_O}{D_R}} \tag{17}$$

and

$$f(t) = D_O \left[ \frac{\partial C_O(x,t)}{\partial x} \right]_{x=0} = \frac{i(t)}{nFA}$$
 (18)

Equation 18 is a statement of Fick's first law where  $\underline{A}$  is electrode area.

Substitution of  $C_{O}(0,t)$  and  $C_{R}(0,t)$  (Equations 15 and 16) into Equation 7d gives

$$c_{O}^{*} - \frac{1}{\sqrt{\pi D_{O}}} \int_{0}^{t} \frac{f(\tau) d\tau}{\sqrt{t - \tau}} = \frac{\gamma S_{\lambda}(at)}{\sqrt{\pi D_{O}}} \int_{0}^{t} \frac{f(\tau) \exp\{-k(t - \tau)\} d\tau}{\sqrt{t - \tau}}$$
(19)

Equation 19 is a linear Volterra integral equation with variable coefficients (16), and represents a succinct statement of the entire boundary value problem. Further operations on Equation 19 are facilitated if it is made dimensionless by the following changes of variable (10)

$$\tau = z/a \tag{20}$$

and

$$f(t) = C_O^* \sqrt{\pi a D_O} \chi(at)$$
 (21)

Equation 19 now takes the dimensionless form,

$$1 - \int_{0}^{at} \frac{\chi(z)dz}{\sqrt{at - z}} = \gamma S_{\lambda}(at) \int_{0}^{at} \frac{\chi(z) \exp\left\{-\left(\frac{k}{a}\right)(at - z)\right\} dz}{\sqrt{at - z}}$$
(22)

The solution of Equation 22 is the function  $\chi(\underline{at})$ . This function depends only on the variable  $\underline{at}$ , which in turn is directly proportional to potential. The relationship between  $\chi(\underline{at})$  and current is (see Equations 18 and 21)

$$i(t) = nFAC_O^* \sqrt{\pi aD_O} \chi(at)$$
 (23)

## Solution of the Integral Equation

Unfortunately, Equation 22 cannot be solved analytically. However, for purposes of subsequent discussions it is useful to examine some limiting cases where analytical solutions can be found. For example, one limiting case occurs when there is no succeeding chemical reaction  $(\underline{k}/\underline{a}=0)$  and  $\underline{\lambda}=0$ . The mechanism for this case is uncomplicated, reversible charge transfer, with an applied potential that has the form of a saw tooth. Under these conditions Equation 22 reduces to

$$\int_{0}^{at} \frac{\chi(z)dz}{\sqrt{at-z}} = \frac{1}{1+\gamma\theta S_{\lambda}(at)}$$
 (24)

where

$$\partial S_{\lambda}(at) = \exp\{at + (\frac{nF}{RT})(E_i - E^0 - E_S)\}$$
 (25)

Equation 24 is an Abel integral equation which has the solution (17)

$$\chi(at) = \frac{1}{\pi\sqrt{at}(1+\gamma\theta)} - \frac{1}{4\pi} \int_{0}^{at} \frac{dz}{\sqrt{at-z} \cosh^{2}(\frac{\ln\gamma\theta+z}{2})}$$
(26)

where

$$\theta = \exp(\frac{nF}{RT})(E_i - E^0 - E_S)$$
 (27)

The definite integral in Equation 26 cannot be expressed in terms of elementary functions, but various common numerical methods can be used to evaluate it (e.g., Simpson's rule).

The first term on the right hand side of Equation 26 is the current-time equation for potentiostatic electrolysis (18). The second term is the current-potential relationship for stationary electrode polarography (10), but because the electrode process is an oxidation the sign for this term is negative. Thus, the overall current for this case is the sum of potentiostatic and linear scan currents. Further, if the potentiostatic current-time curve is used as a base line, the current-potential curve is exactly the same as that obtained for oxidation by linear scan voltammetry with only R initially present. Thus, for example, the value of  $\chi(\underline{at})$  at the peak for this case is -0.446 (10).

A second limiting case for which Equation 22 yields a direct solution is  $\underline{t} < \underline{\lambda}$  when  $(\underline{E_1}/_2 - \underline{E_S})\underline{n}$  is large--i.e. a potential step to the limiting current region for reduction of 0. Under these conditions the right hand side of Equation 22 is negligible, and Equation 22 reduces to

$$\int_{0}^{at} \frac{\chi(z)dz}{\sqrt{at-z}} = 1$$
 (28)

The solution of Equation 28 is easily shown to be

$$\chi(at) = \frac{1}{\pi \sqrt{at}}$$
 (29)

Combination of Equations 23 and 29 gives the expression for current

$$i = \frac{nFA\sqrt{D_O} \quad C_O^*}{\sqrt{\pi t}}$$
 (30)

Equation 30 is the familiar equation for purely diffusion controlled potentiostatic electrolysis under conditions where the surface concentration of substance 0 can be assumed to be zero (18). Under these conditions current clearly is independent of all kinetic parameters, and also is independent of  $\underline{\mathbf{E}}_S$ . Thus, by suitable selection of  $\underline{\mathbf{E}}_S$ , interpretation of theoretical calculations can be simplified.

In general, solutions of Equation 22 including times greater than  $\underline{\lambda}$  can only be obtained numerically. Fortunately Equation 22 is readily amenable to treatment by various numerical methods (10,19). The numerical method of Huber (20) was chosen because it is reasonably straightforward and relatively accurate.

Application of this method to Equation 22 is described in Appendix A, and the FORTRAN computer program is Appendix B. These numerical solutions of Equation 22 were obtained with an accuracy of better than 0.5%.

## Results of Numerical Calculations

Typical results of numerical solution of Equation 22 are shown in Figure 2. Equation 22 contains several variables and in principle the curves of Figure 2 should be a function of all of them. Fortunately, proper specification of experimental conditions permits elimination of some of the variables. In the following discussion the influence of each of the variables of Equation 22 is considered separately.

<u>Effect of E<sub>i</sub></u>. One expects that curves such as those of Figure 2 should be independent of initial potential. This was found to be the case whenever  $(\underline{E}_i - \underline{E}_1/_2)\underline{n}$  was greater than about 150 mv (21). All subsequent data reported here (including those of Figure 2) were calculated for the arbitrary value of  $(\underline{E}_i - \underline{E}_1/_2)\underline{n}$  equal 167 mv, and in this way the parameter  $\underline{E}_i$  was eliminated as a variable.

Effect of  $E_S$ . The derivation of Equation 30 illustrated that if  $E_S$  corresponds to the limiting current region, then the current for  $\underline{t} \leq \underline{\lambda}$  is independent of  $E_S$ . Numerical solutions of Equation 22 for  $\underline{t} \leq \underline{\lambda}$  are described by Equation 30 (within better than 1%) provided the quantity  $(\underline{E}_1/\underline{z} - \underline{E}_S)\underline{n}$  is greater than about 120 mv. For  $\underline{t} > \underline{\lambda}$  the curves are only slightly dependent on  $E_S$ , but even in this case  $E_S$  effectively can be eliminated as a variable in Equation 22 (see discussion under Measurement of Rate

Figure 2. Variation of current function with  $\underline{k}/\underline{a}$  (0.1, 0.05, 0.01) for  $\underline{a}\underline{\lambda}=15$ .

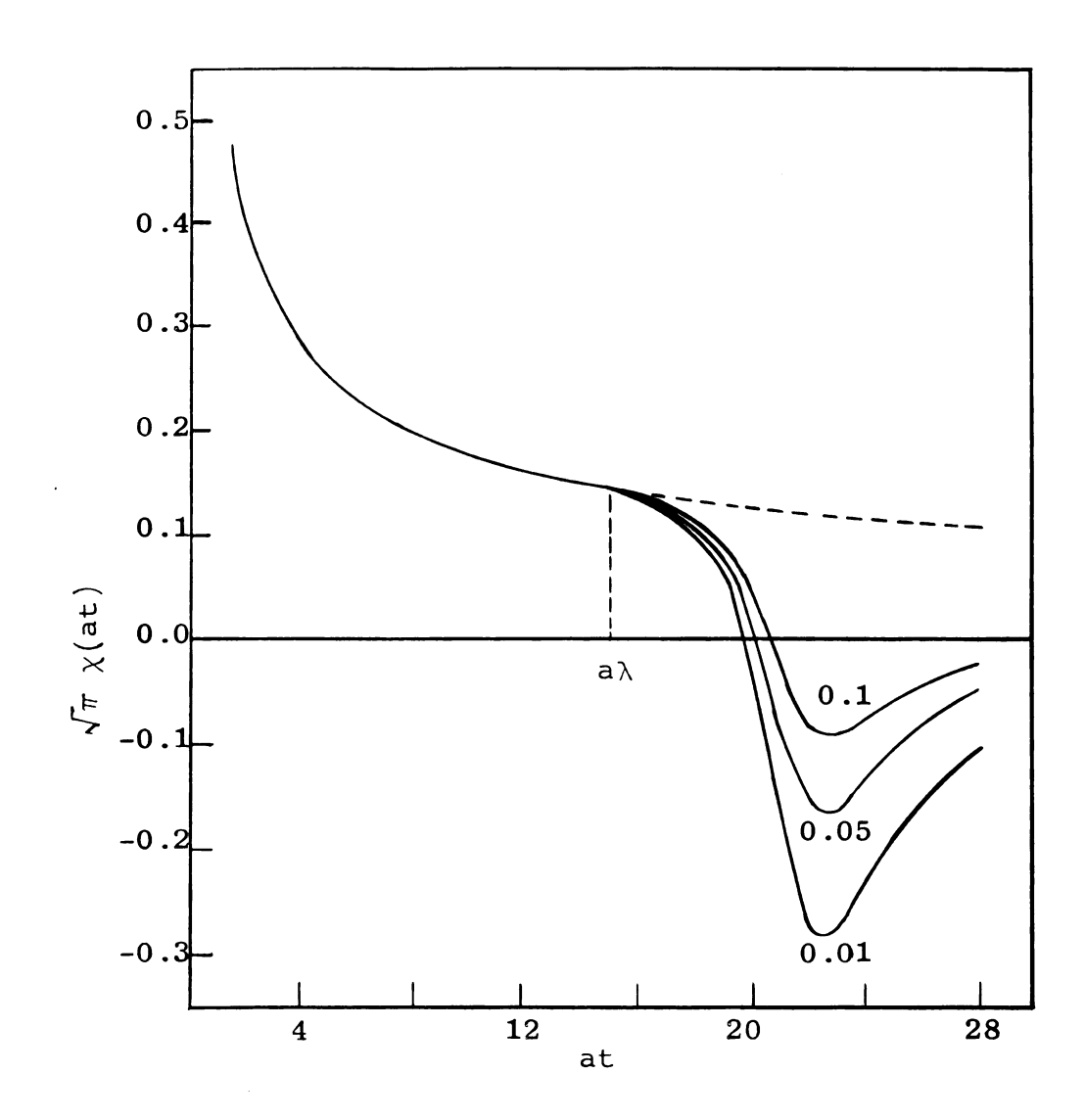


Figure 2

<u>Constants</u>). All calculations reported here were performed with the arbitrary value of  $(\underline{E}_1/_2 - \underline{E}_S)\underline{n}$  equal 167 mv.

<u>Effect of k/a and a\u0388.</u> In general both the parameters  $\underline{k}/\underline{a}$  and  $\underline{a}\lambda$  influence solutions of Equation 22. For example, Figure 2 illustrates the effect of the kinetic parameter  $\underline{k}/\underline{a}$  for a fixed value of  $\underline{a}\lambda$ . Clearly for times less than  $\underline{\lambda}$  the current is independent of  $\underline{k}/\underline{a}$ . This fact is consistent with Equation 30, and is a result of the stepping potential used. As  $\underline{k}/\underline{a}$  approaches zero the linear scan portion of the curve also becomes independent of  $\underline{k}/\underline{a}$  provided measurements are made to the extension of the current-time curve as a baseline. For measurements made in this way the linear scan portion of the curves also is independent of  $\underline{a}\lambda$  in a manner analogous with cyclic voltammetry (10). For example, for small  $\underline{k}/\underline{a}$  the value of  $\sqrt{\pi}\chi_p^*$  always approaches 0.446, which is the same value obtained for cyclic voltammetry in the absence of kinetic complications (10).

For finite values of  $\underline{k}/\underline{a}$  the linear scan portion of the curve is sensitive to changes of  $\underline{k}/\underline{a}$  in two ways. First, the peak potential shifts anodically as  $\underline{k}/\underline{a}$  increases. This behavior is illustrated in Figure 3 where  $(\underline{E}_p - \underline{E}_1/\underline{a})\underline{n}$  is plotted as a function of  $\underline{k}/\underline{a}$  for two values of  $\underline{a}\lambda$ . Although peak potential clearly depends on both  $\underline{k}/\underline{a}$  and  $\underline{a}\lambda$ ,

The new subscript refers to the peak value of the function  $\sqrt{\pi}\chi({ t at})$  measured to the extension of the current-time curve.

Figure 3. Variation of anodic peak potential with  $\underline{k}/\underline{a}$  for  $\underline{a}\underline{\lambda}$  = 0.5 and 62.5.

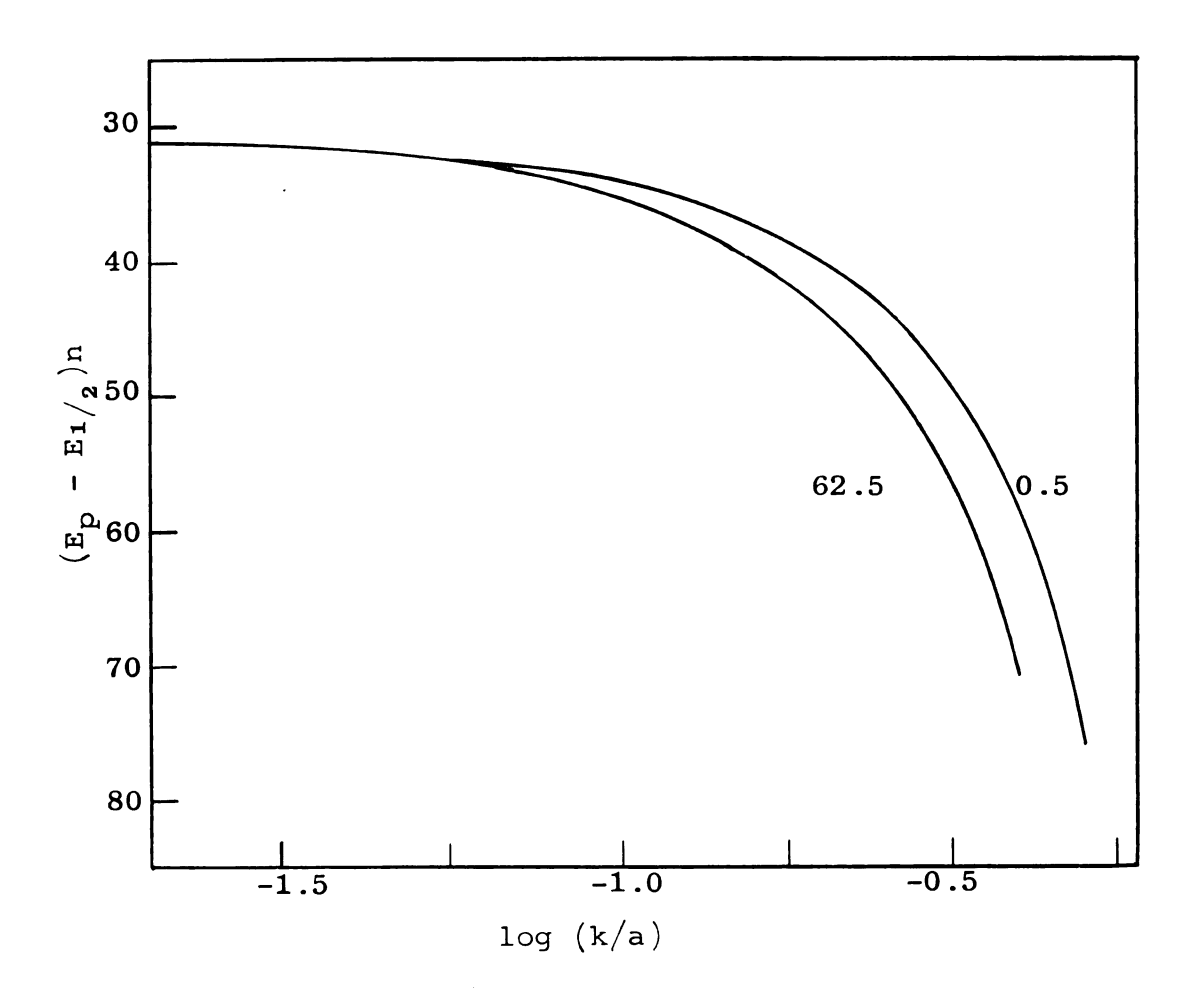


Figure 3

the dependence on  $\underline{a}\underline{\lambda}$  is not great since the values of  $\underline{a}\underline{\lambda}$  represented in Figure 3 correspond to extreme limits.

The second effect of  $\underline{k}/\underline{a}$  is in terms of anodic peak current, and is illustrated in Figures 2 and 4. In Figure 4  $\sqrt{\pi}\chi_p$  is plotted versus  $\underline{k}/\underline{a}$  for several values of  $\underline{a\lambda}$ . In general for fixed  $\underline{a\lambda}$ ,  $\sqrt{\pi}\chi_p$  decreases with increasing  $\underline{k}/\underline{a}$ . The actual magnitude of the peak, however, is a function of both  $\underline{k}/\underline{a}$  and  $\underline{a\lambda}$ . Thus, for fixed  $\underline{k}/\underline{a}$  the size of the anodic peak also decreases with increasing  $\underline{a\lambda}$ . The reason for this effect is that with large  $\underline{a\lambda}$  (constant potential step corresponding to long times) and finite  $\underline{k}/\underline{a}$ , more time is available for the chemical reaction to proceed, and therefore the concentration of unreacted R available for oxidation during the linear scan is less.

From an experimental point of view the fact that  $\sqrt{\pi}\chi_p$  is a function of both  $\underline{a}\lambda$  and  $\underline{k}/\underline{a}$  is particularly important, because this allows adjustment of two experimental parameters,  $\underline{\lambda}$  and  $\underline{v}$ , in such a way as to optimize influence of the kinetics. Thus, to study very fast chemical reactions does not necessarily require large scan rates, because  $\underline{a}\lambda$  can be made small. In this case (see Figure 4, small  $\underline{a}\lambda$ ) kinetic effects are measurable for relatively large  $\underline{k}/\underline{a}$  (i.e. slow scan rates). This situation is in sharp contrast to the work of Schwarz and Shain (11) where their theoretical results are restricted to working with values of  $\underline{k}/\underline{a}$  less than about 0.008. Therefore, to measure the same value of  $\underline{k}$  using the theory of Schwarz and Shain (11) requires scan

Variation of peak current function with k/a for  $a\lambda = 0.5$ , 2.5, 7.5, 20.0, 37.5, and 62.5. Figure 4.

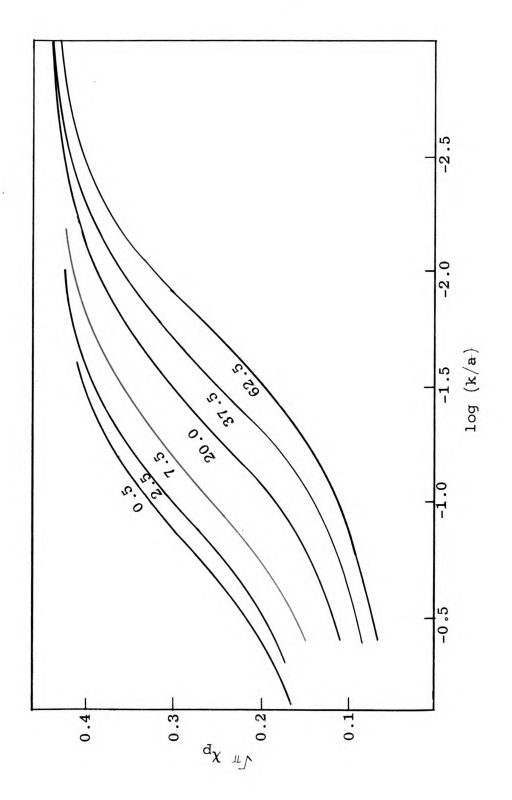


Figure 4

rates approximately 2 orders of magnitude larger than is required using data such as those of Figure 4. An analogous situation exists for measuring small chemical rate constants, where large values of  $\underline{a}\underline{\lambda}$  (see Figure 4) can be selected to provide enhancement of kinetic effects.

Measurement of Rate Constants. To measure rate constants quantitatively, data such as those of either Figure 3 or 4 could be used. From an experimental point of view peak potential shifts are relatively small, and therefore it is preferable to apply the data of Figure 3 as a diagnostic criterion to ensure that the system under consideration conforms with Mechanism I.

As implied in the preceding section, data such as those of Figure 4 are most suitable for quantitative measurement of  $\underline{\mathbf{k}}$ , but to do this experimental values of  $\sqrt{\pi}\chi_{\mathbf{p}}$  must be obtained. This is easily accomplished by recognizing that

$$\sqrt{\pi}\chi_{p} = \frac{i_{p}}{i_{\gamma}} - \frac{1}{\sqrt{\pi a^{\gamma}}}$$
 (31)

where  $\underline{i}_p$  is the experimental peak current (measured to the extension of the current-time curve),  $\underline{i}_\lambda$  is the current at time  $\underline{\lambda}$ , and the remaining terms already have been defined. Thus, data of Figure 4 serve as working curves from which experimental values of  $\underline{i}_p/\underline{i}_\lambda$   $(1/\sqrt{\pi a \lambda})$  can be converted directly to values of  $\underline{k}/\underline{a}$ ; since  $\underline{a}$  is known,  $\underline{k}$  can be calculated. In addition to its simplicity this approach has the advantage that experimental parameters such as  $C_0^*$ ,  $D_0$ ,

A, etc., need not be known. Table I contains numerical values from which working curves like those of Figure 4 can be constructed.

It should be emphasized that the curves of Figure 4 (and data of Table I) are strictly applicable only when  $(\underline{\underline{E}_1}/\underline{2} - \underline{\underline{E}}_s)\underline{n}$  equals 167 mv. Actually the linear scan portion of the curves is not strongly dependent on  $\underline{\mathbf{E}}_{\mathbf{S}}$ , and values of  $(\underline{E}_1/2 - \underline{E}_s)\underline{n}$  within about  $\pm 10$  mv of 167 mv are acceptable. Nevertheless, this fact does constitute a limitation of the method, and therefore an alternate approach was sought. This approach consists of realizing that if a stepping potential more cathodic than -167 mv is used, then an effective  $\underline{\lambda}$ ,  $\underline{\lambda}_{e}$ , can be defined as the time at which the electrode potential during the anodic scan has reached a value of -167 mv with respect to  $\underline{E}_{1/2}$ . This is possible because of the fact that for any potential more cathodic of  $\underline{\underline{\mathbf{E}}}_{\mathbf{1}/\mathbf{2}}$  than -167 mv, the electrode potential always is in the limiting current region and the curve is described by Equation 30 regardless of whether the potential is fixed or is a function of time (22). Because peak potential of the anodic curve is directly proportional to  $\underline{E}_1/_2$  for  $\underline{k}/\underline{a}$  < 0.1 (see Figure 3), in this case  $\underline{\lambda}_{\mathbf{p}}$  is defined as the point  $197/\underline{\mathbf{n}}$  mv cathodic of the anodic peak. If values of k/a greater than 0.1 are encountered the correct estimate of  $\underline{\lambda}_{e}$  can be obtained from Figure 3. Experimentally, then, one simply ensures that  $(\underline{E}_1/_2 - \underline{E}_S)\underline{n}$  is greater than or equal 167 mv, and after the experiment is completed the value of  $\underline{\lambda}_{\mathbf{p}}$  to be used with Figure 4 is determined.

Table I. Variation of  $\sqrt{\pi}\chi_p$  with k/a and  $a\lambda$ .

						аγ					
0.5	5	2.5	5	7.5	5	20		37.5	5	62.5	5
k/a	$\sqrt{\pi}\chi_{\mathbf{p}}$	k/a	$\sqrt{\pi}\chi_{\rm p}$	k/a	$\sqrt{\pi}\chi_{ m p}$	k/a	$\sqrt{\pi}\chi_{\mathrm{p}}$	<b>k</b> /a	$\sqrt{\pi}\chi_{ m p}$	k/a	$\sqrt{\pi}\chi_{ m p}$
0.0250	0.412	0.0100	0.426	0.0067	0.425	0.0010	0.442	0.0010	0.440	0.0010	0.430
0.0400	0.392	0.0200	0.410	0.0133	0.405	0.0030	0.438	0.0027	0.424	0.0024	0.415
0090°0	0.368	0.0400	0.377	0.0267	0.373	0.0050	0.415	0010.0	0.363	0.0050	0.382
0.1000	0.329	0.0600	0.347	0.0400	0.345	0.0100	0 .393	0.0160	0.328	0.0075	0.355
0.1699	0.281	0.0800	0.325	0.0670	0.299	0.0200	0.347	0.0267	0.271	0.0100	0.324
0.2000	0.259	0.1200	0.286	0.1909	0.258	0.0300	0.313	0.0400	0.225	0.0156	0.283
0.2500	0.239	0 ° 3000	0.230	0.1330	0.228	0.0500	0.260	0.0533	0.196	0.0250	0.226
0.4000	0.201	0.3200	0.193	0 .2000	0.191	0.0750	0.216	0.0800	0.159	0.0500	0.155
0.5000	0.185	0.4000	0.183	0.2670	0.172	0.1400	0.160	0.1000	0.140	008000	0.121
0.7500	0.168	0.5000	0.175	0.4000	0.149	0.2500	0.128	0.2000	0.107	0.1500	0.094
						0.4000	0.110	0.4000	280.0	0.4000	0.068

Results of calculations described above extend the versatility of the potential step-linear scan method considerably with respect to the theory of Schwarz and Shain (11). Because application of the rigorous theory is easier than application of the original theory of Schwarz and Shain (11), the potential step-linear scan method now provides a very attractive means of measuring rate constants of chemical reactions initiated electrochemically.

# EXPERIMENTAL EVALUATION OF POTENTIAL STEP-LINEAR SCAN THEORY

To test experimentally the theory of the potential step-linear scan method developed above requires a compound that is reduced (or oxidized) according to Mechanism I, and for which all of the kinetic parameters have been evaluated by an independent method. One compound which satisfies these criteria is azobenzene. A number of previous electrochemical studies (23-33) have established that azobenzene is reduced reversibly in acidic solutions to hydrazobenzene which undergoes the benzidine rearrangement (34).

The benzidine rearrangement is an intramolecular, irreversible reaction, and in the case of azobenzene the rearranged products, benzidine and diphenyline, are not electroactive. Moreover, kinetics of the benzidine rearrangement of hydrazobenzene have been evaluated with several different electrochemical techniques (9.11,35). Thus, azobenzene appeared to be ideally suited to test the theoretical calculations, and evaluate the potential step-linear scan technique.

In addition to testing the theory developed for the potential step-linear scan method, these studies of benzidine rearrangements provided the opportunity to compare homogeneous rate constants measured electrochemically with ones determined by more classical approaches. In spite of the number of cases in which homogeneous rate constants have

been measured electrochemically, there essentially are no examples in the literature where a direct comparison has been made with rate constants measured by accepted classical methods. The major reason for this unusual situation is that the time scales of the two approaches generally do not overlap. Electrochemical techniques are useful for measurements on a much shorter time scale than classical approaches. Thus, provided the electrochemical techniques give meaningful rate constants, the two approaches are complementary. Because of these differences of time scales, comparisons that have been attempted involved an extrapolation of one of the sets of data. For example Schwarz and Shain (9) used the Hammett acidity function to extrapolate electrochemically measured rate constants about two orders of magnitude (toward longer half-lives) to compare them with classical measurements. More recently, Reilley and coworkers (35) applied dielectric constant corrections to classically measured rate constants to provide a comparison with an electrochemically determined constant. Results in both of these cases indicate reasonable agreement between the two approaches. Nevertheless, the uncertainties associated with the various extrapolations leave room for argument that the agreement may have been in part fortuitous.

For these reasons the potential step-linear scan theory also was used to measure rate constants for rearrangement of  $\underline{m}$ -hydrazotoluene. This compound was selected because existing literature data (36) for rate constants measured

spectrophotometrically appeared to provide the best opportunity for comparison of rate constants. An extrapolation of some of the classical data based on dielectric corrections was used, but in addition some of the spectrophotometric experiments were repeated to prove that the extrapolations are valid.

The electrochemical reduction of azobenzene and  $\underline{m}$ -azotoluene on a mercury electrode is complicated by adsorption (11,37). Although the potential step-linear scan technique has the advantage that adsorption effects are reduced, for generation times much greater than the half-life of the chemical reaction, anomalous surface phenomena were observed. The addition of gelatin to solutions of these compounds reduced these effects so that longer generation times could be used. To justify using gelatin a study of its effect on the reduction of azobenzene also was made.

#### EXPERIMENTAL

### Instrumentation

Ohmic potential losses are a possible source of serious error in all of the electrochemical measurements made in this study. Generally, correction for these ohmic potential losses cannot be accomplished by simply applying Ohm's law (38). However, by using a three electrode potentiostatic circuit it is possible to compensate electronically for a majority of the potential loss. Figure 5 is a block diagram of the potentiostatic circuit which was used to accomplish this compensation.

The control amplifier (C.A.) is a high gain differential amplifier which employs negative feedback to maintain the difference of potential between the inverting (-) and non-inverting (+) inputs at zero volts. Since the sum of the potentials in the comparison loop (inverting input, reference electrode (R.), working electrode (W.), function generator (F.G.) and noninverting input) is zero, any potential of the function generator will be imposed between the reference and working electrodes.

Two different control amplifiers were employed, a commercial instrument (Wenking Potentiostat, Model 61RS, Brinkmann Instruments, Westbury, N.Y.), and one constructed from operational amplifiers and a booster (Philbrick Researches, Inc., Dedham, Mass., Model P45AU and P66A (booster)). No distinction could be made between experimental results

# Figure 5. Circuit diagram of potentiostat with floating load resistor.

C.A. : Control amplifier
(-) : Inverting input
(+) : Noninverting input
R. : Reference electrode
W. : Working electrode
C. : Counter electrode
F.G. : Function generator

D. ; Detector

 $\mathbf{R_{L}}$  : Load resistor

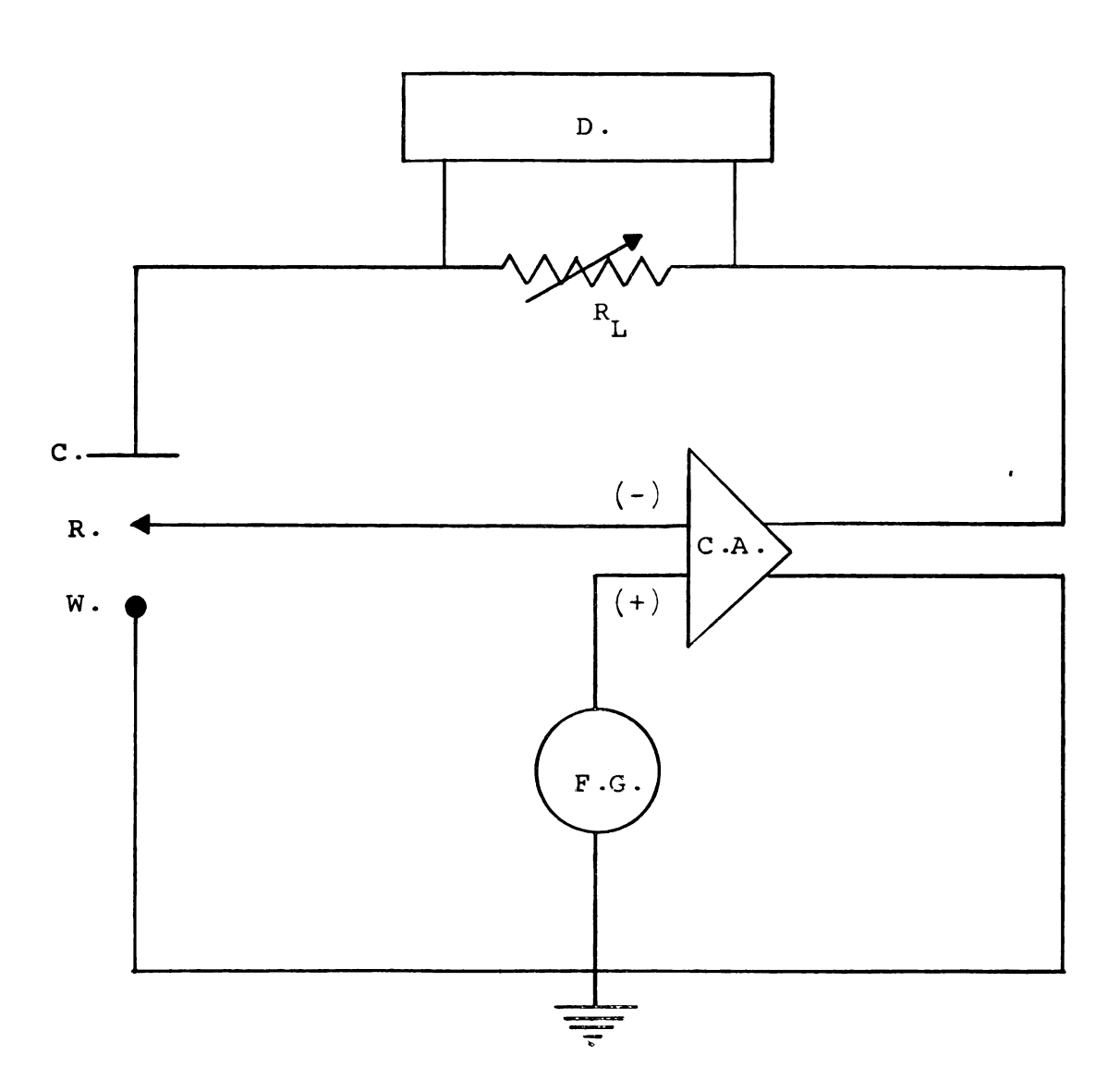


Figure 5

obtained with either instrument.

Cell current was determined from the potential drop across the load resistor,  $\underline{R}_{r}$ . To measure this potential drop two different recording devices were used depending on the time scale of the experiment. For experiments lasting less than about 1 sec a storage oscilloscope (Tektronix, Inc., Beverton, Ore., Type 564 with 2A63 (vertical) and 2B67 (horizontal) plug-in units) with Polaroid camera attachment (Tektronix Type C-12) was employed. For longer electrolyses an x-y recorder (Honeywell, Inc., San Diego, Calif., Model 520) was used. Both these recording devices have differential inputs which are well isolated from ground so that  $\underline{iR}$  drop across the floating load resistor could be measured easily, and the circuit of Figure 5 functioned satisfactorily. However, for some early experiments a potentiometric recorder (Leeds and Northrup, Model G) was employed. This recorder cannot be operated differentially, and therefore for this recorder the circuit of Figure 5 had to be modified. A block diagram of the modified circuit is given in Figure 6. Basically this circuit is the same as the one in Figure 5, but an additional amplifier is added to act as a current follower (39)(C.F.). This current follower maintains the potential of the working electrode at virtual ground, and thereby eliminates introduction of iR potentials into the control loop. At the same time the output of the current follower relative to ground potential is equal to  $\underline{iR}_{t}$  , so that one side of the detector can be grounded.

Figure 6. Circuit diagram of modified potentiostat.

C.A. : Control amplifier
(-) : Inverting input
(+) : Noninverting input
R. : Reference electrode
W. : Working electrode
C. : Counter electrode
F.G. : Function generator

D. : Detector

C.F. : Current follower
R<sub>I.</sub> : Load resistor

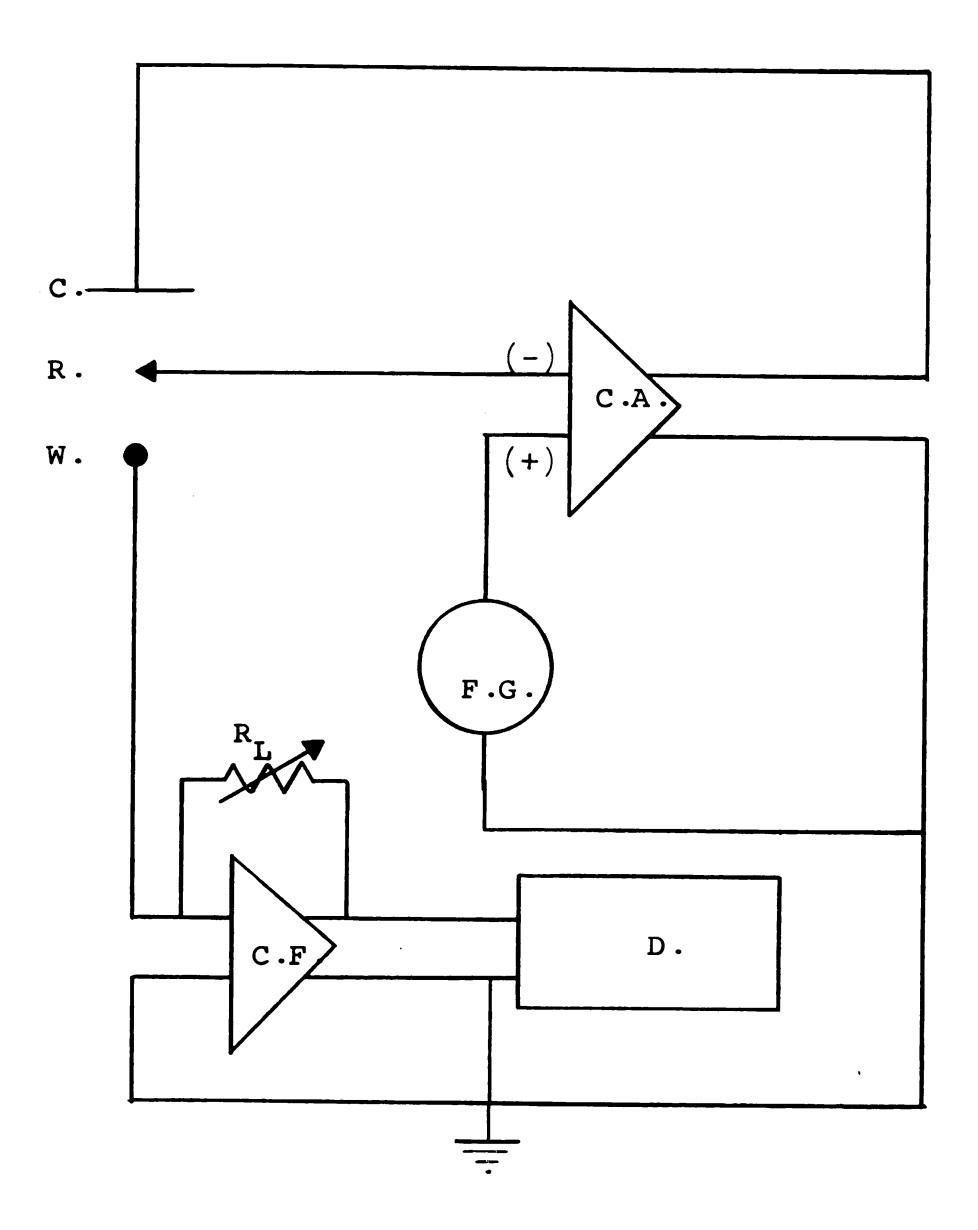


Figure 6

The various electrochemical techniques used in this study (polarography, cyclic voltammetry, potentiostatic electrolysis and potential step-linear scan electrolysis) require different potential-time functions. For cyclic voltammetry and polarography this function (triangular wave) was obtained from a commercial function generator (Exact Blectronics, Inc., Hillsboro, Ore., Model 255). For potentiostatic electrolysis a battery operated low voltage power supply was used to generate the gate. The function for the potential step-linear scan technique was obtained by summing via a passive adding network a delayed triangular wave with a gate of opposite polarity from the low voltage power supply. The triangular wave was obtained from the function generator, which contains an internal delay mechanism so that it is possible to trigger the function generator with the gate, making  $\lambda$  easily variable. With this function generator scan rates from 0.001 to 1,000 Hz with a maximum amplitude of 2 volts could be dialed directly.

Polarograms were obtained with a Sargent Model XV Polarograph.

For the spectrophotometric measurements a Beckman Model DB was used.

The cell arrangement is shown in Figure 7. The cell consists of a glass weighing bottle with a 60/12 % joint on the top. The cell lid is made of Teflon and machined to fit this joint. Holes were drilled in the lid to allow insertion of the various cell components (Figure 7).

## Figure 7. Cell arrangement.

: Reference electrode Α

: Scoop В

Hanging mercury drop electrode
Dropping mercury electrode
Deoxygenator
Counter electrode C

D

E

F

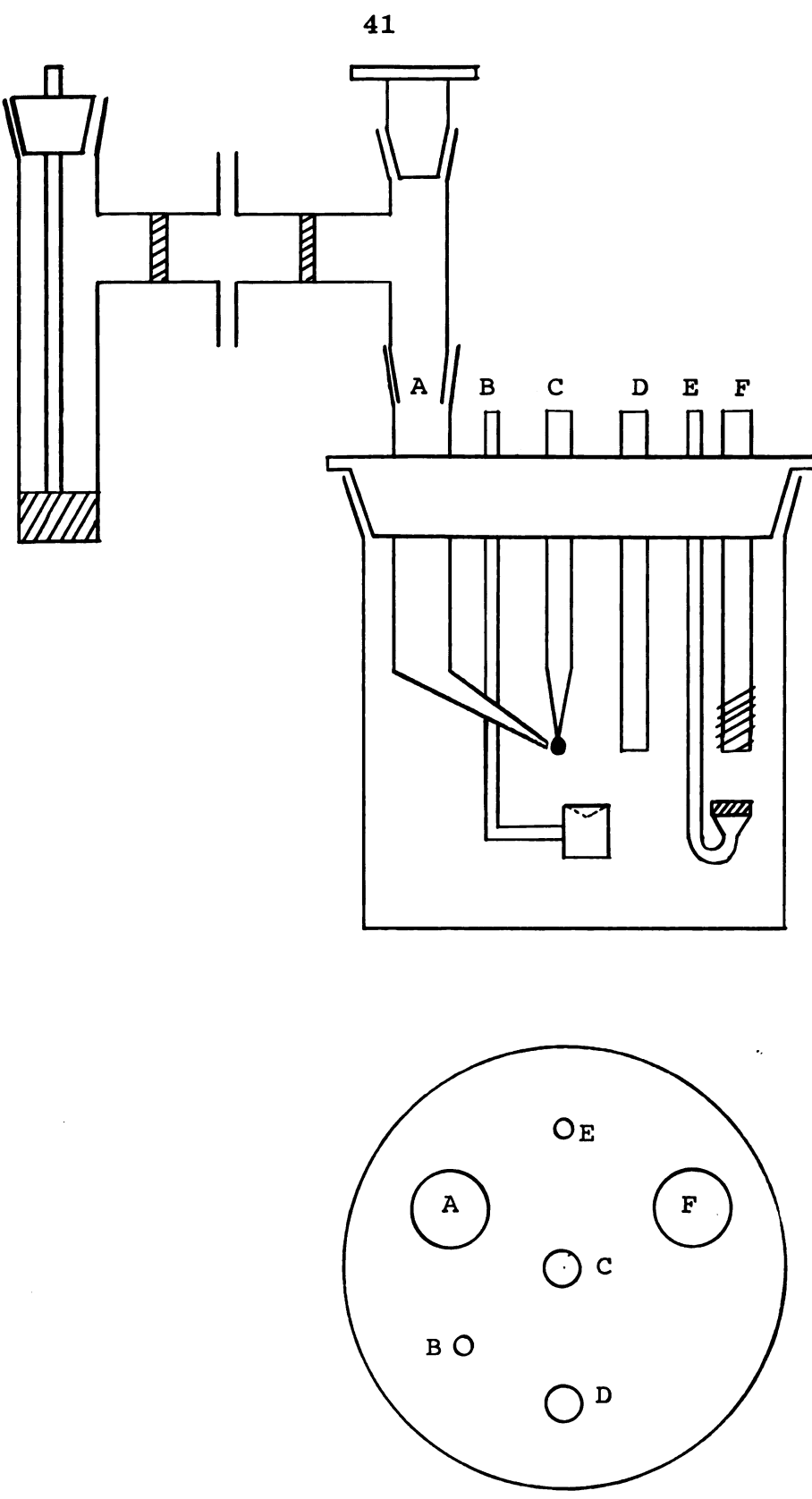


Figure 7

The counter electrode consists of platinum wire (1 foot, number 26 gauge) wound around 6 mm soft glass tubing. One end of the platinum was sealed in the glass tubing, and electrical contact was made through mercury contained in the glass tubing.

The reference electrode contained three separate sections separated by 10 mm fine fritted glass discs. The left hand compartment (Figure 7) was a saturated calomel electrode, and the right hand compartment contained the solution being investigated. Because the latter solution contained perchlorate, 1M sodium nitrate was used in the middle compartment to prevent precipitation of potassium perchlorate. Liquid junction potentials obviously arise when different solutions are contacted in this manner. However, in this work only relative potential measurements were necessary. Presumably the liquid junction potential for a given solution would remain constant during the course of an experiment. In fact, half-wave potentials for a given system never varied more than about 10 mv over the course of the entire investigation. The right hand compartment of the reference electrode could be disassembled at the 14/20 joint so that either a Luggin capillary or a tube closed with a 10 mm fritted glass disc could be used to contact the solution. The Luggin capillary was constructed so that it could be positioned within less than 1 mm of the surface of the working electrode. In this way uncompensated ohmic potential losses always were less than one ohm.

For experiments requiring a stationary electrode, a hanging mercury drop constructed in the manner described by Ross, DeMars and Shain (40) was used. Generally three mercury drops from the dropping mercury electrode (Sargent S-29419 capillary, 2-5 sec) were collected in a scoop and suspended from the working electrode. The area of this electrode was  $0.085 \pm 0.001$  cm<sup>2</sup> for all acid concentrations.

The deoxygenator was of conventional design and could be raised above the solution to provide a nitrogen blanket over the solution while measurements were being made.

All measurements were made in a constant temperature room at ambient temperature of  $23-24^{\circ}\text{C}$ .

Chemicals. Zone refined azobenzene (Litton Chemicals, Inc., Fernandina Beach, Fla.) was used without further treatment. m-Azotoluene was prepared by reduction of m-nitrotoluene with zinc dust and sodium hydroxide (41). The product was purified by eluting it with petroleum ether (30-60°) from an alumina column, followed by repeated recrystallizations from ethanol. Melting point (54°C, uncorrected) and infrared spectra agreed with the literature.

Anal. Calcd. for C14H14N2: C, 79.97; H, 6.71; N, 13.32.

Found: C, 80.06; H, 6.69; N, 13,36. m-Hydrazotoluene was prepared by reduction of the m-azotoluene (36).

<u>Procedures</u>. For electrochemical experiments procedures and preparation of solutions were identical with the description of Schwarz and Shain (9,11) except that to avoid air

oxidation of the  $\underline{m}$ -azotoluene, solvents were deaerated prior to dissolving the  $\underline{m}$ -azotoluene. The solvent for all experiments was 50% (by weight) ethanol-water. As in the work of Schwarz and Shain no attempt was made to maintain constant ionic strength, because the salt effect in 50% ethanol is small (9).

In general for spectrophotometric measurements the procedure of Carlin and Odioso (36) was followed exactly. The one exception was that because the half-life of the reaction being studied was fairly small (ca. 70 sec.), the quenching procedure of Carlin and Odioso (36) could not be employed. The procedure used consisted of rapid mixing of a solution of the m-hydrazotoluene in 50% ethanol with a solution of perchloric acid in 50% ethanol, followed by rapid transfer to the spectrophotometer cell. These operations were easily completed within one half-life of the chemical reaction. Absorbance was then recorded directly as a function of time with a potentiometric recorder. Analysis of these absorbance-time data followed the procedure of Carlin and Odioso (36).

### RESULTS AND DISCUSSION

## Effects of Gelatin

Both azobenzene and hydrazobenzene adsorb on mercury (11,35,37). Most electrochemical studies of this system, however, have been performed at relatively low acid concentration (23-33) (pH = 2-13), where the extent of adsorption is small, and the rate of the benzidine rearrangement is slow with respect to duration of the experiment.

Holleck and co-workers (30-32) investigated effects of surface active materials on the polarographic behavior of azobenzene and hydrazobenzene in  $0.1\underline{\text{M}}$  perchloric acid. They concluded that gelatin became adsorbed on the electrode and inhibited the electron transfer reaction. Nygard (27) made similar studies using other electrochemical techniques, and his results generally agree with Holleck and co-workers.

Using potentiostatic electrolyses, Schwarz and Shain (11), also reported an anomalous stirring effect which occurred at high acid concentration. This effect was evidenced by large periodic fluctuations in current-time curves; qualitatively the time at which this happened appeared to be proportional to the rate of the benzidine rearrangement.

Results of these previous investigations indicate that gelatin has two main effects. First, gelatin is preferentially adsorbed, which largely eliminates adsorption of depolarizer. Second, adsorbed gelatin inhibits the rate of

the heterogeneous electrode reaction. Even if the electron transfer rate is inhibited, however, it often may still be possible to select experimental conditions where the electron transfer is reversible. Under such conditions the second effect of gelatin cited above should be unimportant. and the only effect of gelatin would be to eliminate adsorbtion of depolarizer and reaction products. In this case measurements of homogeneous kinetic parameters on systems where adsorption is prevalent should be improved by using Because if these conclusions are correct they would have not only important bearing on the present investigation, but on the study of chemical reactions coupled to electrode processes in general, a number of experiments were performed in an effort to define exactly the role of gelatin. Results of these experiments are described in the following paragraphs.

The effects of gelatin on reduction of azobenzene were investigated using four techniques: conventional polarography, cyclic voltammetry, chronoamperometry, and potential step-linear scan electrolysis. Conventional polarographic studies were made with solutions of about 1 mm azobenzene with perchloric acid concentration from 0.5m to 1.0m, and 0.00 to 0.05% gelatin. Results of these experiments are summarized in Table II. No meaningful data could be obtained in the absence of gelatin, because of extensive stirring phenomena which apparently are related to adsorption of depolarizer, and which increase with increasing acid concentration

Table II. Polarographic data for the reduction of azobenzene at various gelatin and acid concentrations.

$C_{O}^{*}, \underline{mM}$	[H <sup>+</sup> ), <u>M</u>	Gelatin,%	$i_{\tau}$ , $\mu$ amp	$i_{L}/c_{O}^{*}$ x103	$\frac{\mathbf{E_1^a}}{2}$ v
				_ Г. О	
1.000	0.500	0.00	6.17		
0.980	0.490	0.01	5.58	5.70	0.025
0.962	0.481	0.02	5.39	5.63	0.025
0.943	0.472	0.03	5.28	5.61	0.024
0.926	0.463	0.04	5.16	5.57	0.024
0.909	0.455	0.05	5.10	5.62	0.024
1.000	1.00	0.00			
0.980	0.98	0.01	5.76	5.87	0.059
0.962	0.96	0.02	5.52	5.76	0.062
0.942	0.94	0.03	5 <b>.3</b> 9	5.73	0.062
0.926	0.93	0.04	5.22	5.64	0.061
0.909	0.91	0.05	5.25	5.77	0.061
1.000	1.50	0.00			
0.980	1.47	0.01			
0.962	1.44	0.02	5.64	5.86	0.095
0.942	1.41	0.03	5.45	5.78	0.096
0.926	1.39	0.04	5.40	5.82	0.096
0.909	1.36	0.05	5.25	5.77	0.095
1.000	2.00	0.00			
0.980	1.96	0.01			
0.962	1.93	0.02	5.70	5.92	
0.943	1.89	0.03	5.57	5.92	0.132
0.926	1.85	0.04	5.45	5.90	
0.909	1.82	0.05	5.34	5.87	

<sup>&</sup>lt;sup>a</sup>Half-wave potentials are <u>versus</u> S.C.E.

(see Figure 8). However, for higher gelatin concentrations the normalized limiting current,  $i_L/c_0^*$ , is a constant within experimental error for all acid concentrations. Moreover, values of  $\underline{E}_1/_2$  appear to be independent of gelatin concentration. This last fact implies that even if gelatin does decrease the rate of the electron transfer reaction, this reaction is still rapid enough to be reversible under polarographic conditions.

Cyclic voltammetry also was used to study the effect of gelatin on anodic and cathodic peak currents in approximately 0.5M perchloric acid. With cyclic voltammetry rate constants for a succeeding chemical reaction can be determined from the ratio of anodic to cathodic peak currents In addition rate constants for rearrangement of hydrazobenzene in 0.5M perchloric acid are accurately known Thus, it is possible to measure rate constants with cyclic voltammetry in solutions both with and without gelatin present, and to compare these rate constants with the known values. Results of these experiments, which are listed in Table III, show very good agreement between the known and measured rate constants. Normalized cathodic peak current,  $i_p/c_0^*$ , decreases slightly when gelatin is added, presumably because preferentially adsorbed gelatin reduces the amount of weakly adsorbed azobenzene (37). At higher acid strengths than 0.5M it is impossible to make kinetic measurements without gelatin present because of the stirring phenomena cited in relation to the polarographic experiments (Figure 9).

Figure 8. Conventional polarographic current-potential curves showing effects of gelatin on reduction of azobenzene.

1mM azobenzene, 0.5M perchloric acid.

A, no gelatin;

B, 0.02% gelatin;

 $1_{\underline{M}\underline{M}}$  azobenzene,  $1.0\underline{M}$  perchloric acid.

C, no gelatin;

D, 0.02% gelatin.

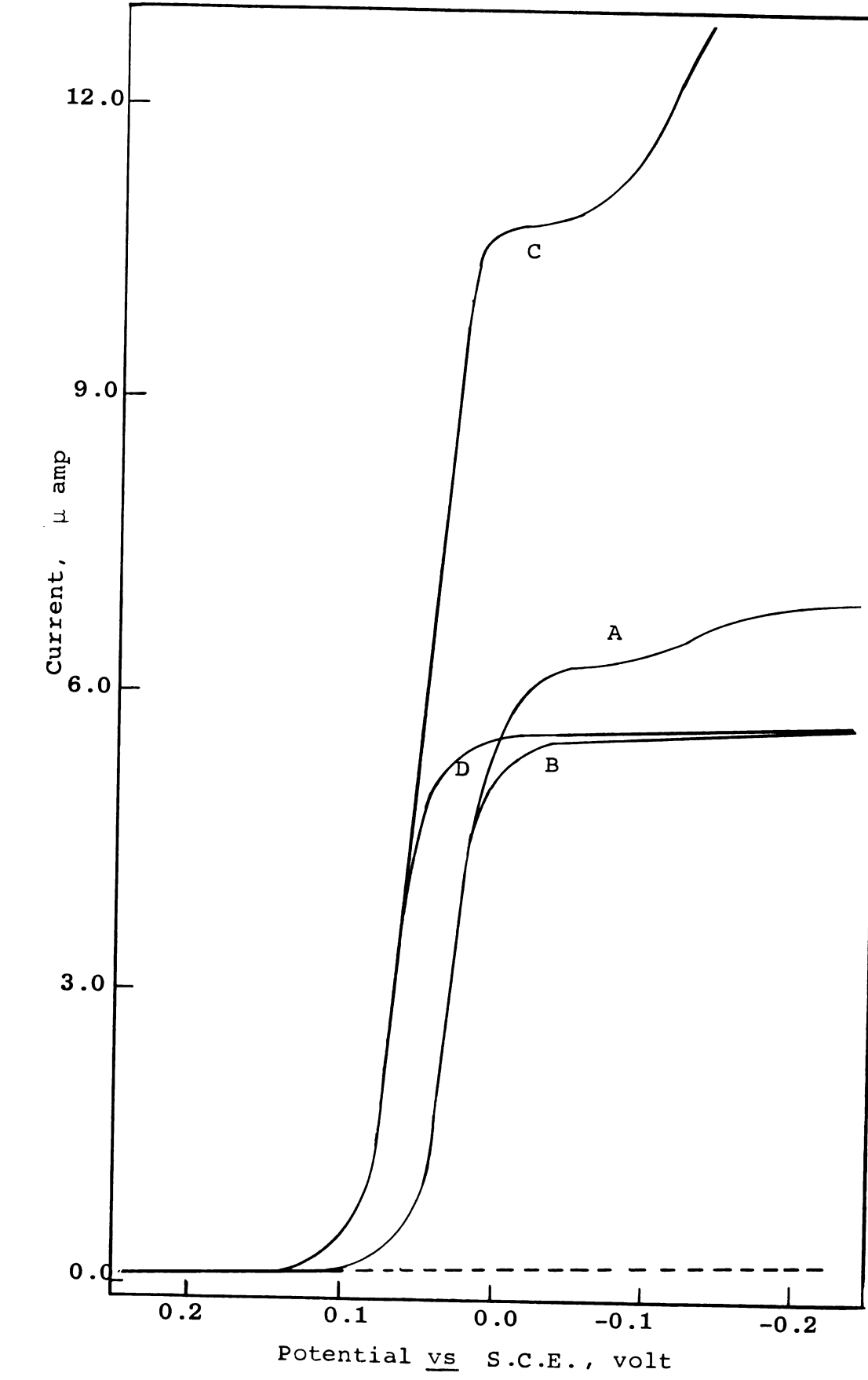


Figure 8

Table III. Comparison of rate constants for rearrangement of hydrazobenzene determined with and without gelatin present.

$C_0^*, \underline{mM}$	<u>м</u> , [+н]	Gelatin,%	$\frac{i_p/c_0^*}{}$	$\frac{k}{2}$ sec. $a$	$\frac{k}{}$ sec. $\frac{1}{}^{b}$
1.000	0.500	0.00	0.023	0.204	0.204
0.980	0.490	0.01	0.022	0.192	0.256
0.962	0.481	0.02	0.022	0.181	0.187
0.943	0.472	0.03	0.022	0.172	0.180
0.909	0.455	0.05	0.022	0.156	0.160

aRate constants determined by Schwarz and Shain in the absence of gelatin (9).

Rate constants determined with cyclic voltammetry using ratio of anodic to cathodic peak currents.

- Figure 9. Stationary electrode polarograms showing effects of gelatin on reduction of  $\underline{m}\underline{M}$  azobenzene (scan rate, 30 mv sec^-1.
  - A, 0.5-2.0<u>M</u> perchloric acid, 0.02% gelatin.
  - B, 1.0M perchloric acid, no gelatin.
  - C,  $2.0\overline{\underline{M}}$  perchloric acid, no gelatin.

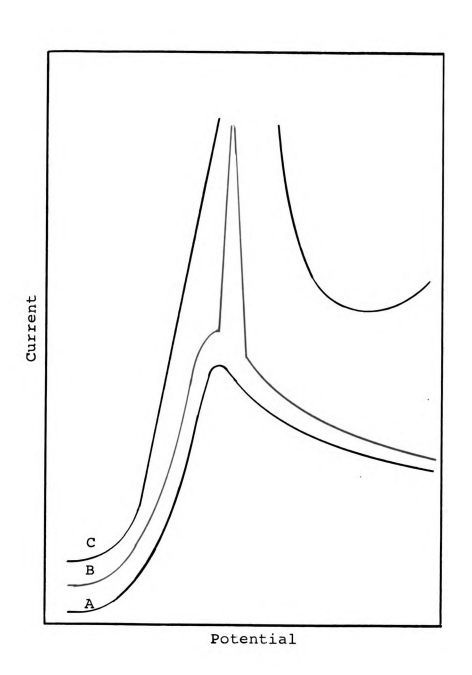


Figure 9

The effect of gelatin on diffusion coefficients was determined by calculating diffusion coefficients from potentiostatic electrolysis data. This technique was chosen because adsorption effects of depolarizer are minimized and thus the effect of gelatin adsorbed on the electrode surface could be evaluated. Solutions of about 1mM azobenzene, approximately 0.5 and 2.0M perchloric acid, and from 0.00 to 0.05% gelatin were employed. Data were analyzed by the conventional plot of i versus  $1/\sqrt{t}$ , and results are listed in Table IV. Clearly, from these data the measured diffusion coefficient is not affected by the presence of gelatin. There may, however, be a small influence of ionic strength since the values of  $D_0$  are slightly higher in  $2.0\underline{M}$ perchloric acid. The average diffusion coefficient of all values in Table V is  $3.3 \times 10^{-6} \text{ cm}^2 \text{ sec}^{-1}$ . A value of  $3.4 \times 10^{-6}$  cm<sup>2</sup> sec<sup>-1</sup> was determined by Schwarz and Shain (9) for measurements in the absence of gelatin.

For potentiostatic experiments, the same stirring effect reported by Schwarz and Shain (see Figure 10), and mentioned above in connection with polarographic and cyclic voltammetric experiments, was observed. As in the case of polarography and cyclic voltammetry this effect is eliminated for any acid concentration when at least 0.02% gelatin is present.

Very recently, Wopschall and Shain (37) treated theoretically the effects of adsorption processes on single-scan and cyclic stationary electrode polarograms. Based on their

.

.

.

Table IV. Diffusion coefficients of azobenzene for different acid and gelatin concentrations.

				b
$C_0^*, \underline{MM}$	[H <sup>+</sup> ], <u>M</u>	Gelatin,%	Slope <sup>a</sup>	$\begin{array}{ccc} D_{02} \times 10^{6} \\ CM^{2} & sec^{-1} \end{array}$
1.000	0.500	0.00	16.3	3.1 ± 0.1
0.980	0.500	0.01	16.0	3.1 ± 0.1
0.943	0.500	0.03	15.7	3.2 ± 0.1
0.909	0.500	0.05	15.1	3.2 ± 0.1
1.000	2.00	0.00	16.9	3.3 ± 0.1
0.980	2.00	0.01	16.7	3.4 ± 0.1
0.943	2.00	0.03	16.3	$3.5 \pm 0.1$
0.909	2.00	0.05	15.3	$3.3 \pm 0.1$

<sup>&</sup>lt;sup>a</sup>Slope determined from plot of <u>i</u> versus  $1/\sqrt{t}$ .

bError level is average deviation of three experiments.

Chronoamperometric curves showing effects of gelatin on reduction of azobenzene. Figure 10.

A,  $0.5-2.5\underline{M}$  perchloric acid, 0.02% gelatin. B,  $1.0\underline{M}$  perchloric acid, no gelatin.

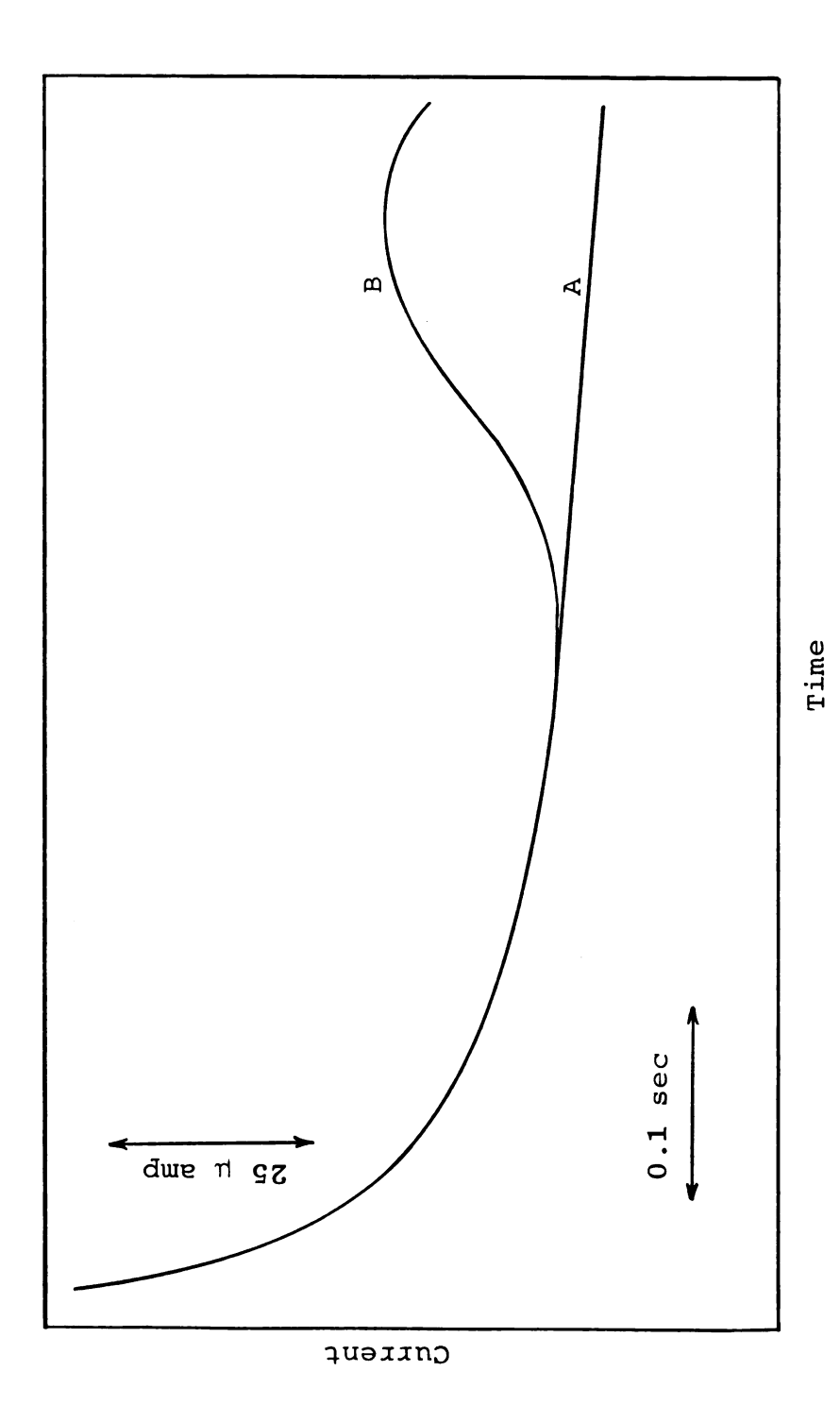


Figure 10

theoretical results and the experimental results already discussed, the azobenzene system appears to fit a model where in the absence of gelatin weak adsorption of both azobenzene and hydrazobenzene occurs. However, gelatin apparently is preferentially adsorbed, and therefore in the presence of gelatin adsorption of azobenzene and hydrazobenzene is essentially eliminated. Also gelatin slows the rate of the electron transfer, but the effect is not great, and conditions easily can be selected where the process remains reversible.

Because the potential step-linear scan method is a combination of cyclic voltammetry and potentiostatic electrolysis, the effects of gelatin on this method should be a combination of effects already discussed for the latter two methods. Experimental results, which indicate that this is the case, are discussed in the following section along with applications of the potential step-linear scan theory.

## Reduction of Azobenzene

To check the theoretical calculations for the potential step-linear scan method, the azobenzene system can be used because of the extensive electrochemical data already available (9,11,35). Experimental conditions were arbitrarily selected identical with those of Schwarz and Shain (9). In general the azobenzene system was found to behave exactly as described by Schwarz and Shain (9,11). The one exception

is that gelatin does tend to eliminate the anomalous stirring behavior Schwarz and Shain observed when electrolysis
times are longer than the half-life of the chemical reaction.

As shown below, the presence of gelatin does not have a
significant effect on rate constants measured by potential
step-linear scan.

In Figure 11 experimental and theoretical potential step-linear scan curves for azobenzene are compared. experimental curve (solid line) actually corresponds to two different experiments, one in which gelatin was employed (0.02%), and another in which gelatin was not used. These two curves are within experimental error and therefore are represented by a single line. The theoretical currents (circles) were calculated from Equation 22 using  $a\lambda = 10.4$ ,  $\underline{n}$  = 2.0,  $C_O^*$  = 1.0 $\underline{m}\underline{M}$  and the diffusion coefficient determined by Schwarz and Shain (9) of  $3.4 \times 10^{-6}$  cm<sup>2</sup> sec<sup>-1</sup>. To obtain the comparison between theoretical and experimental curves the value of k/a in the theoretical calculations was varied to give the best fit. Clearly the agreement between theory and experiment is excellent. However, it might be argued that the reason for this agreement is the adjustable parameter, k/a, which was selected to give the best agreement. To answer this question it is necessary to determine if the value of k which gives best agreement with theory is the correct rate constant for the chemical reaction. Therefore, an evaluation of rate constants determined by the potential step-linear scan theory is discussed next.

- Figure 11. Comparison of theory and experiment for potential step-linear scan method.
  - o, theory  $(\underline{a\lambda} = 10.4, \underline{k}/\underline{a} = 0.03)$
  - —, experimental for reduction of  $\underline{\text{mM}}$  azobenzene in  $0.5\underline{\text{M}}$  perchloric acid. Scan rate, 94 mv sec  $\frac{E_1}{\lambda}$ , 0.024 v vs S.C.E.; A, 0.085 cm²; and  $\frac{\lambda}{\lambda}$ , 1.42 sec.

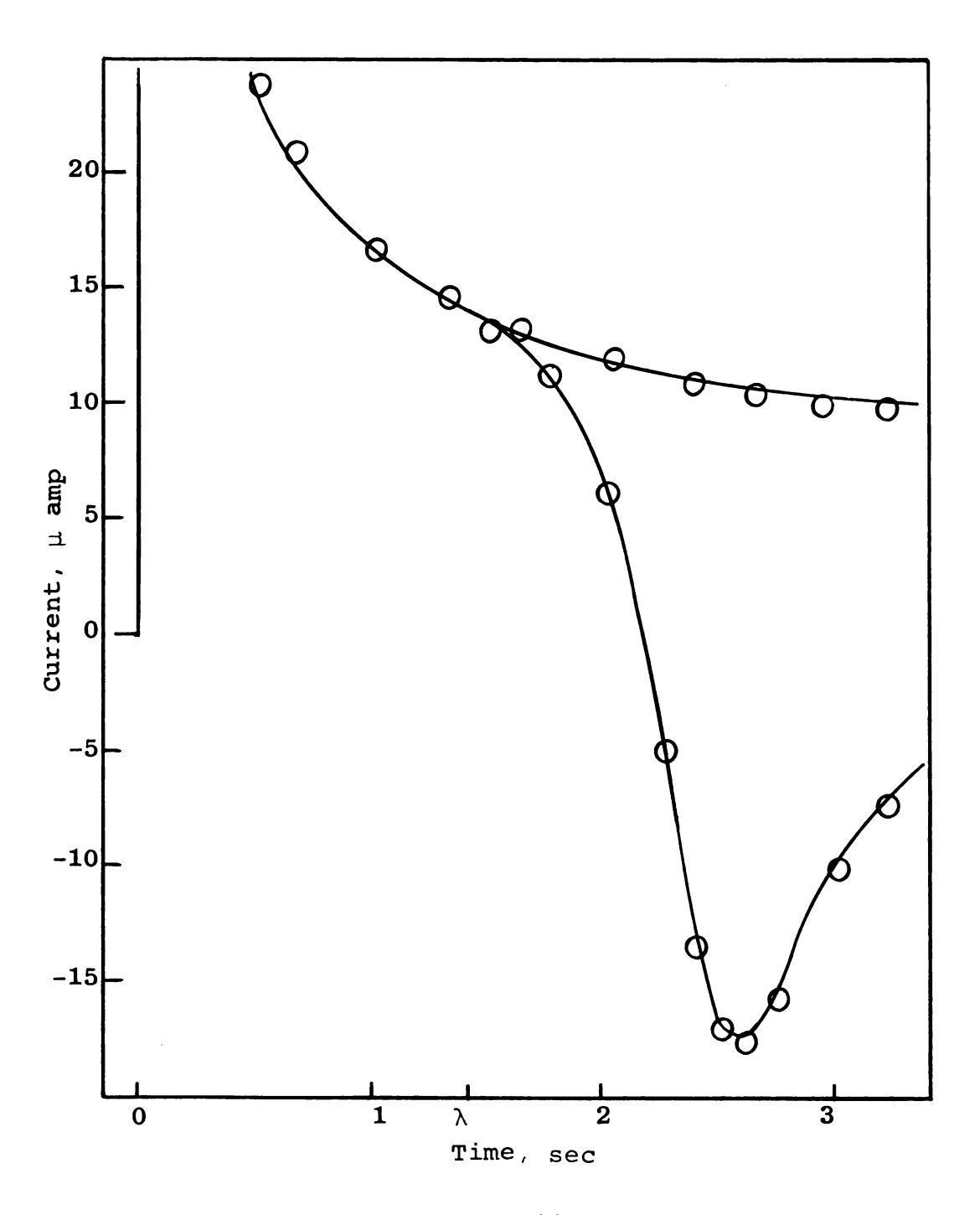


Figure 11

The fact that rate constants determined with the aid of the working curves discussed above (Figure 4) agree with rate constants determined by an independent electrochemical method is illustrated in Figure 12\*. In Figure 12 circles represent rate constants determined with the potential steplinear scan theory developed above. Each circle corresponds to measurements both with and without gelatin; results in the two cases are within experimental error. Nevertheless with gelatin present much larger values of  $\underline{\lambda}$  could be used than in the absence of gelatin. The squares of Figure 12 represent rate constants determined by Schwarz and Shain (9).

With the potential step-linear scan method it was possible to cover as wide a range of rate constants as Schwarz and Shain reported for the squarewave technique (9). Moreover, the range is considerably greater (in the direction of large rate constants) than Schwarz and Shain studied with their potential step-linear scan theory (11) (the largest rate constant they report is  $\log(\underline{k}) = 0.4$ ). Although not stated explicitly by Schwarz and Shain the reason for this upper limit was no doubt set by the approximations of their theory. Thus, for them to measure larger rate constants, and still satisfy the assumptions of their theory, would have required prohibitively large scan rates where effects of adsorption, double layer charging, and charge transfer kinetics become dominant.

At high acid concentrations in 50% ethanol the Hammett acidity function,  $H_0$ , must be used as a measure of acidity, rather than the molarity of the acid. Values of  $H_0$  in Figure 12 were obtained from the paper of Schwarz and Shain (9).

Figure 12. Variation of  $\underline{k}$  with  $\underline{H}_0$  for the benzidine rearrangement of hydrazobenzene.

- O, potential step-linear scan method.  $\Box$ , squarewave electrolysis (9).

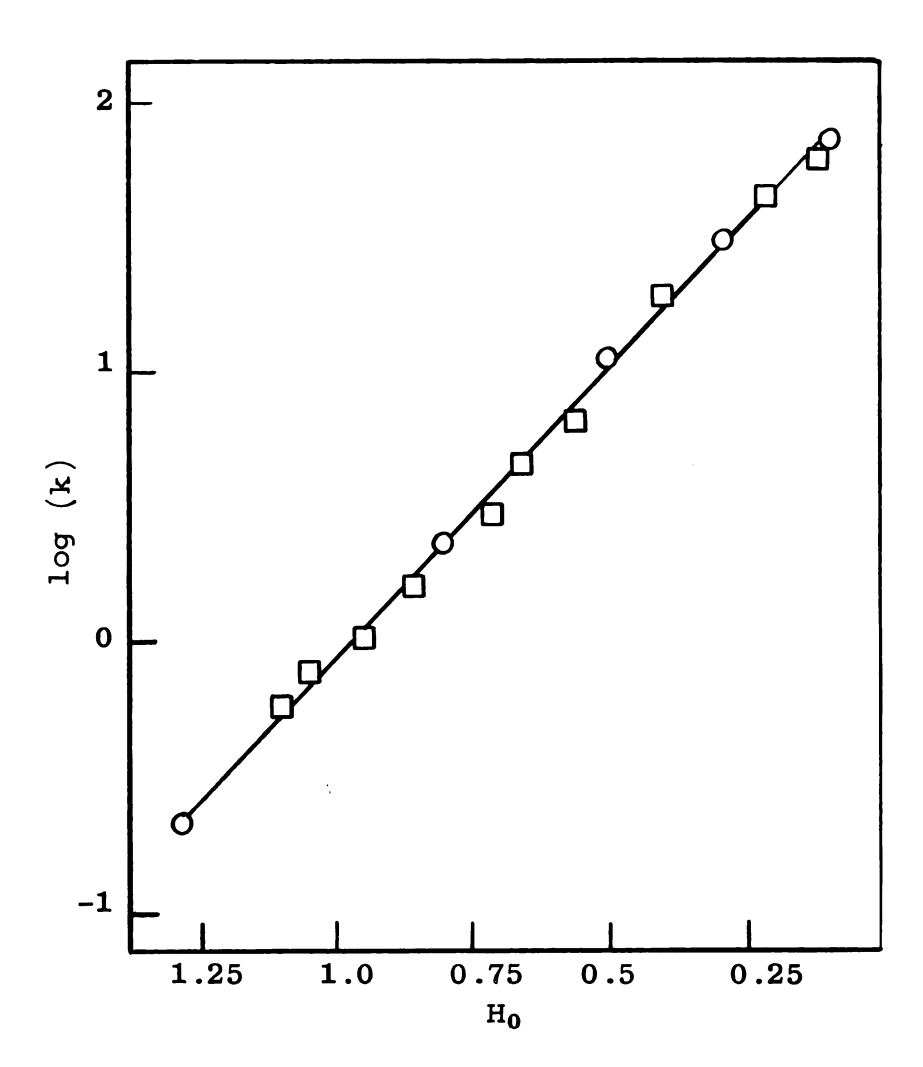


Figure 12

# Reduction of m-Azotoluene

The potential step-linear scan method also was used to study the reduction of m-azotoluene. Qualitatively this system behaves the same as azobenzene. Some differences were observed, however. For example, the anomalous behavior reported by Schwarz and Shain (11) for long electrolysis times was even more pronounced than with azobenzene. As with azobenzene it was found that gelatin minimized this effect without affecting the value of measured rate constants. Most of the data reported for m-azotoluene were obtained with 0.01% gelatin. Another difference between m-azotoluene and azobenzene is reversibility of the electrode reac-Thus, under identical experimental conditions (without gelatin) the apparent heterogeneous rate constant for azobenzene is a factor of 2 or 3 larger than for m-azotoluene. This effect presumably is related to structural differences in the two compounds, and is discussed in more detail in a later section. The final major difference between the two compounds is the rate of the benzidine rearrangement. At identical acid concentrations, m-azotoluene rearranges roughly 5 times faster than azobenzene. This effect is well known and explained by the inductive influence of the methyl groups.

Rate constants determined for rearrangement of  $\underline{m}$ -hydrazo-toluene are summarized in Table V, and are plotted against acid concentration\* in Figure 13 (circles). The slope of

For these acid concentrations it is not necessary to use the Hammett acidity function.

Table V. Rate constants for rearrangement of  $\underline{m}$ -hydrazo-toluene.

Acid Conc. , M			
0.05	0.0067; 0.0059		
0.06	0.0126 <sup>C</sup>		
0.07	0.0133		
0.08	0.0177	0.021 ± .003	
0.10	0.035	0.036 ± .003	
0.20		0.138 ± .004	
0.30		0.329 ± .007	
0.40		$0.769 \pm .017$	

aFor rate constants in the second column the acid was hydrochloric (however, see footnote c); in the third column the acid was perchloric.

bExtrapolated values of Carlin and Odioso (36).

<sup>&</sup>lt;sup>C</sup>For spectrophotometric measurements under electrochemical conditions 0.010 and 0.015 sec<sup>-1</sup> were obtained.

Rate constants measured by potential step-linear scan.
Numbers in parentheses are average deviations of at least
12 experiments.

Figure 13. Variation of  $\underline{k}$  with concentration of perchloric acid for rearrangement of  $\underline{m}$ -hydrazotoluene.

- O, potential step-linear scan method.
- spectrophotometric technique (36).
  determined spectrophotometrically under electrochemical conditions.

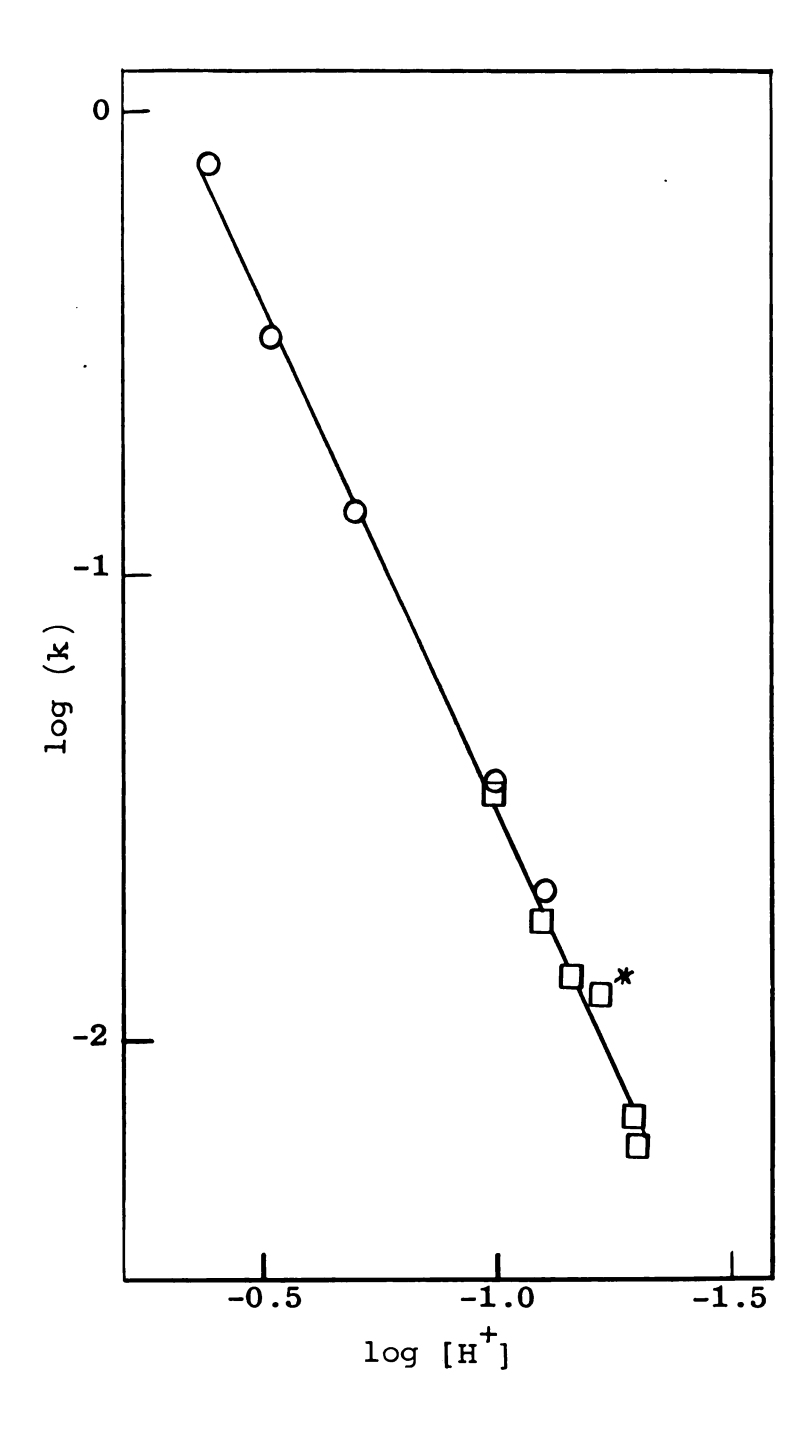


Figure 13

the straight line drawn in Figure 13 is 2.16 which is consistent with the well-known second order dependence of benzidine rearrangements on acid concentration.

Comparison of rate constants. Rate constants for rearrangement of m-hydrazotoluene have been determined spectrophotometrically by Carlin and Odioso (36), and it is possible to compare these results with the electrochemical results reported above. Unfortunately the classical measurements were performed under different experimental conditions where the rate of the reaction is slower (lower temperature and lower dielectric constant solvent--95% ethanol rather than the 50%). Nevertheless the dependence of rate constant on dielectric constant and temperature is known (36, 42), and therefore it is possible to extrapolate the rate constants of Carlin and Odioso to the electrochemical experimental conditions. This same procedure was used by Reilley and co-workers (35), who for one specific acid concentration found reasonably good agreement between extrapolated classical and electrochemical measurements. Rate constants of Carlin and Odioso extrapolated to conditions used in the electrochemical experiments also are included in Figure 13 (squares) and Table V. The agreement between the two approaches is excellent, and appears to justify the extrapolation. In spite of this a number of criticisms can be raised against the extrapolation procedure, and it might be argued that the agreement of Figure 13 is at least partly

fortuitous. To test this possibility the measurements of Carlin and Odioso were repeated for one acid concentration, but for the same solvent and other experimental conditions employed for the electrochemical measurements (see discussion under <a href="Experimental">Experimental</a>). The rate constant determined in this way is identical within experimental error with the extrapolated value (see Figure 13 and Table V). Thus, the extrapolation is valid, and one concludes that at least for the mechanism and time scale considered here homogeneous rate constants can be measured electrochemically with complete confidence.

#### REDUCTION OF AZOBENZENE IN N.N-DIMETHYLFORMAMIDE

After using azobenzene compounds to evaluate the potential step-linear scan theory, it was of interest to attempt to determine the mechanism of the electrode reaction itself. Studies with the potential step-linear scan technique all were performed under conditions where the electrode reaction was completely reversible. However, it is possible to make electrochemical measurements under conditions where the electrode reaction is perturbed away from equilibrium, and in this way kinetics of the electrode reaction can be measured.

Preliminary heterogeneous kinetic studies in water indicated a 2-electron reduction involving hydrogen ions. Because of the complications resulting from hydrogen ion these aqueous data were not readily interpretable, and it was concluded that studies of the reduction mechanism of azobenzene in an aprotic solvent might profitably aid interpretation of aqueous data. N,N-Dimethylformamide (DMF) was chosen because a considerable number of electrochemical studies have been made in this solvent. Although DMF is not an aprotic solvent, studies (43) have shown the proton availability is small. Results of the non-aqueous studies are discussed first, and the aqueous work constitutes the final part of this thesis.

During the course of this investigation Aylward, Garrett, and Sharp (44) published a report on the reduction of

azobenzene in DMF with  $0.1\underline{M}$  tetraethylammonium perchlorate supporting electrolyte. These authors used conventional d.c. and a.c. polarography. In addition, controlled potential electrolysis was used to determine  $\underline{n}$  values, and ESR spectroscopy was used to examine reduction products.

Their results show that azobenzene is reduced in two one electron steps. The first electron addition occurs at a value of  $\underline{E}_1/_2$  of -1.81 v and the second at  $\underline{E}_1/_2$  of -2.29 v versus a silver-silver nitrate reference electrode. An ESR spectroscopic study showed that the product of the first electron transfer is the monoanion of azobenzene, and the product of the second electron transfer is diamagnetic. Alternating current polarography and faradaic impedance measurements indicated that the first electron transfer is rapid with a heterogeneous rate constant of 0.51  $\pm$  0.05 cm sec<sup>-1</sup>, and the second electron transfer is irreversible. They postulated that the product of the second step is the dianion of azobenzene. The diffusion coefficient for azobenzene in DMF was found to be 7.7  $\pm$  0.3 x 10<sup>-6</sup> cm<sup>2</sup> sec<sup>-1</sup>.

The independent studies of azobenzene in DMF with cyclic voltammetry reported in this thesis are in essential agreement with the work of Aylward, Garrett, and Sharp.

The work of this investigation actually complements the results of Aylward and co-workers, and where appropriate, comparisons between the two studies are made.

Although the original objective of studying the reduction of azobenzene in aprotic solvent was to aid interpretation

of aqueous data, because of the unambiguous nature of the mechanism found in DMF, these studies also offered the opportunity of studying effects of molecular structure on reactivity. A number of correlations between half-wave potential (thermodynamic correlations) and structure have been reported in the literature. In spite of this apparently no correlations between reactivity--i.e., heterogeneous rate constant of the electrode reaction--and structure have been made. By studying the reduction kinetics in DMF of a series of substituted azobenzene compounds, some correlations between reactivity and structure were possible. Although preliminary in nature results of these studies are of interest and also are described.

#### EXPERIMENTAL

#### <u>Instrumentation</u>

Circuits and cells were identical with those already discussed in connection with experimental applications of the potential step-linear scan theory.

## Materials

<u>Solvent</u>. Fisher certified reagent grade N,N-dimethylformamide (DMF) was used as solvent without further purification. The specific conductivity was  $1.4 \times 10^{-6}$  (ohm cm)<sup>-1</sup> which is about one order of magnitude larger than values reported by Thomas and Rochow (45) for "Pure" DMF. Conductivity measurements were made for solutions containing 0.1, 0.2, and 0.3 $\underline{\text{M}}$  tetraethylammonium perchlorate (supporting electrolyte) to obtain an estimate of the uncompensated resistance. The resulting conductivities were 0.0056, 0.0093 and 0.0126 (ohm cm)<sup>-1</sup> respectively.

Chemicals. 4,4'-Diethylazobenzene, 2,2'-, 3,3'- and 4,4'- dimethylazobenzene were prepared by reduction of the corresponding nitro compounds with sodium hydroxide, methanol and zinc dust (41). p-Ethylnitrobenzene was prepared by mononitration of ethylbenzene (46). The fraction boiling at 126°C and 13 mm (46) was used for the reduction.

- 4,4'-Dibromoazobenzene, 4,4'-dichloroazobenzene and 4,4'-dinitroazobenzene were prepared from the corresponding p-aniline by oxidation with silver iodide dibenzoate in anhydrous benzene (47), followed by repeated recrystallization from ethanol and acetone.
- 4,4'-Bis(acetamido)azobenzene and 4,4'-diaminoazobenzene were prepared from p-aminoacetanilide (48).
- 1,1'-Azonaphthalene was obtained from K and K Laboratories Inc., Plainsview, N.Y.-Hollywood, Calif. and 4,4'-azobis(N,N-dimethylaniline) was obtained from Eastman Organic Chemicals, Rochester, N.Y.

The observed melting points for the various compounds are listed in Table VI.

Tetraethylammonium perchlorate was prepared by metathesis of tetraethylammonium bromide with sodium perchlorate (49). The product was recrystallized six times from distilled water and dried at  $66^{\circ}$ C.

## Procedures

<u>Solutions</u>. Solutions were prepared by dissolving accurately weighed samples of the appropriate azo-compound and tetraethylammonium perchlorate in enough DMF for a final solution volume of 100 ml. These solutions were generally about  $4 \times 10^{-4} \underline{\text{M}}$  in azo-compound, and  $0.3\underline{\text{M}}$  in tetraethylammonium perchlorate.

Table VI. Comparison of observed and literature values for melting points of substituted azobenzene compounds.

Compound	M.P. <sup>a</sup> , OC	M.P b,0C	
Azobenzene	68	68	(24)
4,4'-Bis(acetamido)azobenzene	288	288-293dec	.(48)
4,4'-Diaminoazobenzene	238-239	<b>238-241</b> dec	.(48)
4,4'-Dibromoazobenzene	205	203-205	(47)
4,4'-Dichloroazobenzene	184	184-185	(47)
4,4'-Diethylazobenzene	59-60	59-60	(61)
2,2'-Dimethylazobenzene	55-56	55	(62)
3,3'-Dimethylazobenzene	54-55	55	(63)
4,4'-Dimethylazobenzene	141-142	142	(47)
4,4'-Dinitroazobenzene	224-225	223-225	(47)

a<sub>Observed</sub> melting point.

b<sub>Literature</sub> melting point, reference in parentheses.

Evaluation of Diffusion Coefficients. Diffusion coefficients were evaluated from cyclic voltammetry experiments with scan rates sufficiently slow that the couple under investigation was reversible (see diagnostic criteria for reversibility in reference (10)). Under this condition the expression (10) relating diffusion coefficient to the cathodic peak current,  $i_p$ , is

$$\sqrt{D_0} = \frac{i_p}{268 \text{ n}^{3/2} \text{ A C}_0^* \sqrt{v}}$$

For these experiments  $\underline{A}$  and  $\underline{v}$  were 0.0621 cm<sup>2</sup> and 0.630 volts/sec respectively, and the bulk concentration of azocompound was approximately 1.0mm. The supporting electrolyte was  $0.3\underline{M}$  tetraethylammonium perchlorate.

Evaluation of  $E_1/_2$ . Values of  $E_1/_2$  for azo-compounds also were determined with cyclic voltammetry. Again, scan rates were such that the couple was reversible. Under this condition the value of  $E_1/_2$  is the potential at 85.14% of the cathodic peak current (10).

Measurement of Heterogeneous Rate Constants. Heterogeneous rate constants,  $\underline{k}_s$ , for substituted azobenzene compounds also were determined from cyclic voltammetric data. This approach involves using scan rates sufficiently large that the electrode reaction is perturbed from equilibrium, which is indicated by an overpotential between cathodic and anodic peak potentials  $(\underline{\triangle E}_p)$ . Recent theoretical calculations

(14) provide the quantitative relationship between  $\Delta E_p$ , scan rate, and the rate constant,  $\underline{k}_s$ . These theoretical relationships are presented in the form of a working curve, which is a plot of  $\underline{n} \times \Delta E_p$  against a dimensionless parameter,  $\underline{\psi}$ . The parameter  $\underline{\psi}$  has the value  $\underline{\gamma}^\alpha \underline{k}_s / \sqrt{\pi a D_0}$ , where  $\underline{\gamma}$  is  $(D_0/D_R)^{1/2}$ ,  $\underline{\alpha}$  is the transfer coefficient, and other terms were defined earlier. Thus, to use this approach to measure  $\underline{k}_s$ , a large plot of the working curve was constructed, and this plot was used to relate experimental  $\Delta E_p$  values to  $\underline{\psi}$ . Since scan rate was accurately known, values of  $\underline{k}_s$  could be calculated from  $\underline{\psi}$ , provided  $\underline{\gamma}$  and  $\underline{\alpha}$  were known.

Actually, for the large organic molecules studied here, with both oxidized and reduced forms soluble in solution,  $D_0$  and  $D_R$  are nearly the same. Moreover,  $\underline{\alpha}$  is usually about 0.5, and therefore, it is reasonable to assume that the quantity  $\underline{\gamma}^{\alpha}$  is nearly unity. This approximation was made in all measurements of  $\underline{k}_{\underline{\alpha}}$ .

The working curve described above was calculated for  $\underline{\alpha}$  = 0.5; for different values of  $\underline{\alpha}$  a different working curve results. Fortunately, however, for large values of  $\underline{\psi}$  all working curves are independent of  $\underline{\alpha}$ . For example, for  $\underline{\psi}$  = 0.1 there is about a 20% difference of  $\underline{\Delta E}_p$  for  $\underline{\alpha}$  between 0.3 and 0.7, but for larger  $\underline{\psi}$  the variation rapidly becomes less. Therefore, to minimize this source of error, scan rates were selected to correspond to values of  $\underline{\psi}$  always larger than 0.5, and in this way errors resulting from inaccurate knowledge of  $\underline{\alpha}$  were at most 5% (14).

For all experiments the initial potential was at least 160 mv anodic of  $\underline{E_1}/_2$ , and switching potential was about 140 mv cathodic of  $\underline{E_1}/_2$ . Switching potential is not critical as long as it is reasonably near the  $141/\underline{n}$  mv used in theoretical calculations of the working curve (14).

Although the use of cyclic voltammetry to measure heterogeneous rate constants in the manner just described is very simple and convenient, a serious source of error is uncompensated ohmic potential losses (iR drop). This is because of the fact that uncompensated iR drop causes "apparent" overpotentials which vary with scan rate in approximately the same way as activation overpotentials (38). Thus, it is essential that the uncompensated iR drop be small and known. To minimize uncompensated resistance, the 3-electrode circuits already discussed were used in conjunction with a Luggin capillary reference probe which was placed in close proximity with the working electrode (< 1mm). In addition, a relatively high concentration of supporting electrolyte was used to increase conductivity (0.3M tetraethylammonium perchlorate), and a relatively low concentration of depolarizer  $(4.0 \times 10^{-4} \text{M})$  was used to minimize cell current. Under these conditions the largest cell currents encountered were about 0.1 ma, and based on the conductivity measurements, and the discussion of Booman and Holbrook (50), the maximum uncompensated iR loss was about 1 mv.

#### RESULTS AND DISCUSSION

Cyclic voltammetric data for azobenzene confirm the results of Aylward and co-workers. A typical cyclic polarogram for reduction of azobenzene is shown in Figure 14. The first wave corresponds to a one electron reversible electron transfer as is evident from the peak potential separation of approximately 60 mv (10) and the value of about 60 mv for the quantity  $(\underline{E}_{p/2} - \underline{E}_p)$  (10). The second wave corresponds to an irreversible one electron addition. The peak potential separation for the two cathodic waves is about 500 mv.

Actually, cyclic polarograms of 4,4'-, 3,3'- and 2,2'-dimethylazobenzene, 4,4'-dichloroazobenzene, 4,4'-dibrom-azobenzene, 4,4'-diethylazobenzene and 1,1'-azonaphthalene are identical in all important aspects with curves for azobenzene. Thus, curves of Figure 14 can be considered representative of all of the above compounds. Based on these results it was concluded that all of these compounds are reduced by the same mechanism as azobenzene--i.e., the mechanism of Aylward and co-workers.

The reduction of 4,4'-dinitroazobenzene is complicated because nitro groups are reduced at about the same potential as the azo-linkage. Because in DMF the nitro reduction also occurs in steps, it is difficult to determine exactly which wave corresponds to reduction of the azo group. Furthermore, difficult base line corrections would have to be applied

Figure 14. Cyclic stationary electrode polarogram for reduction of  $\underline{m}\underline{M}$  azobenzene in  $0.3\underline{M}$  tetraethylammonium perchlorate and N,N-dimethylformamide (scan rate, 40 v sec $^{-1}$ ).

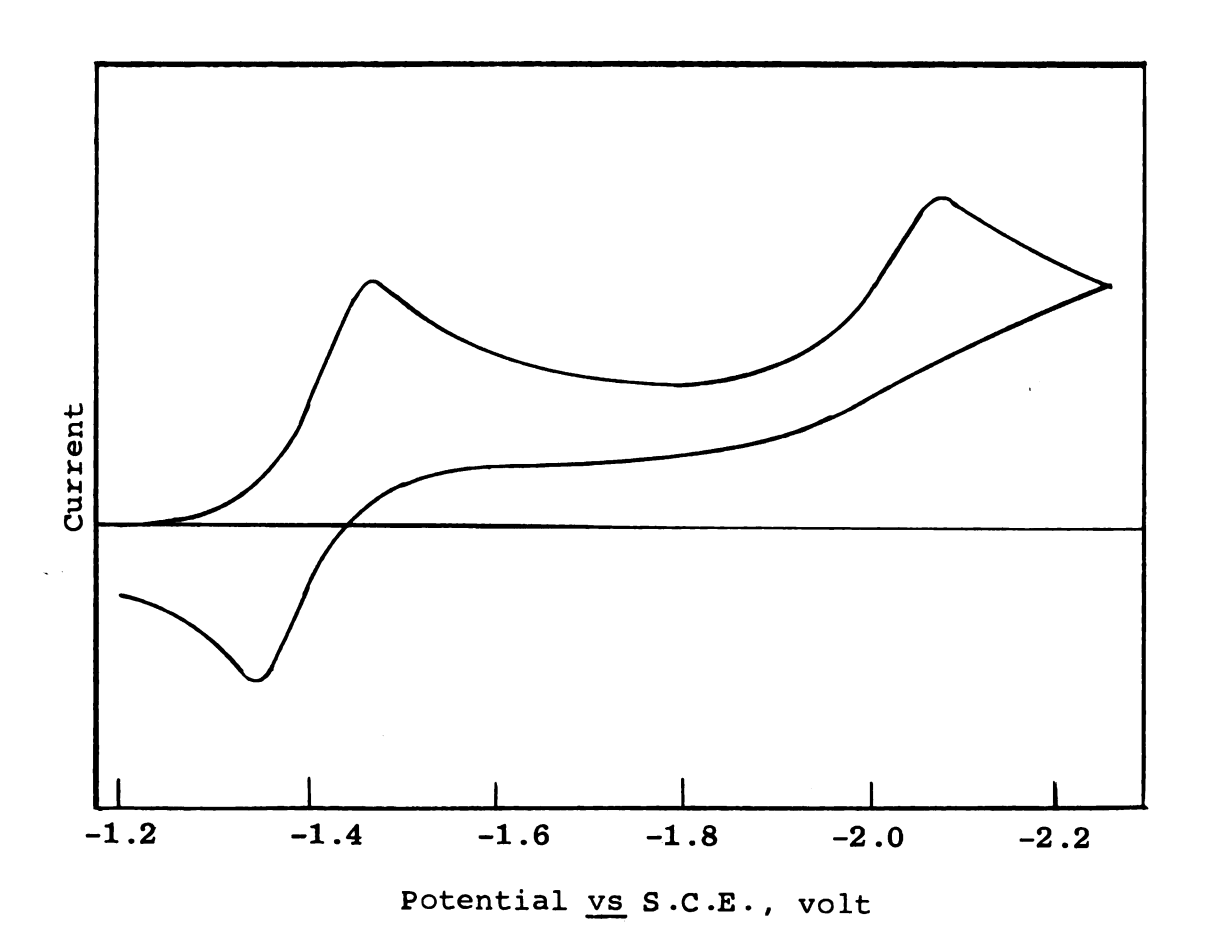


Figure 14

to obtain quantitative information. For these reasons this system was not investigated further.

4,4'-Azobis(N,N-dimethylaniline), 4,4'-diamino- and 4,4'-bis (acetamido)azobenzene also show deviation from the results obtained for azobenzene. Two waves are observed in the cyclic voltammetry current potential curves. However, the first wave is broader  $[(\underline{E}_{p/2} - \underline{E}_{p})]$  is about 80 mv], and the anodic current is considerably reduced even at very large scan rates (ca. 100 volts/sec). A second wave also is observed at more cathodic potentials, however, it occurs at a potential only about 150 mv cathodic of the first. A mechanism where the product of the first electron transfer disproportionates to give starting material and the product reduced at the second wave is consistent with these results, but no detailed study was made.

## Evaluation of Diffusion Coefficients

To calculate values of  $\underline{k}_s$  from the parameter  $\underline{\psi}$  (see discussion under Experimental) it is necessary to know accurately the diffusion coefficient,  $\underline{D}_0$ , for the oxidized form of depolarizer. Therefore, diffusion coefficients in DMF were determined for all azobenzene compounds on which heterogeneous kinetic measurements were made. Results of these measurements are summarized in Table VII.

Comparison of Measured Diffusion Coefficients with

Stokes-Einstein Diffusion Theory. It is interesting to note

Table VII. Diffusion coefficients of substituted azobenzene compounds in N,N-dimethylformamide.

Compound	ip'	$C_0^*, \underline{mM}$	D <sub>0</sub> x 10 <sup>6</sup> cm <sup>2</sup> sec <sup>-1</sup>	(M.W.)
Azobenzene	36.8	1.000	$7.8 \pm 0.2^{b}$	0.177
1,1'-Azonaphthalene	34.3	1.009	$6.7 \pm 0.2$	0.154
4,4'-Dibromoazobenzene	32.8	1.000	$6.2 \pm 0.2$	0.143
4,4'-Dichloroazobenzene	34.3	1.010	$6.7 \pm 0.2$	0.158
4,4'-Diethylazobenzene	33.9	0.981	$6.9 \pm 0.2$	0.161
2,2'-Dimethylazobenzene	35.5	0.990	$7.3 \pm 0.2$	0.168
3,3'-Dimethylazobenzene	34.8	0.970	$7.4 \pm 0.2$	0.168
4,4'-Dimethylazobenzene	35.0	0.985	$7.3 \pm 0.2$	0.168

<sup>&</sup>lt;sup>a</sup>Error level is average deviation of six experiments.

<sup>&</sup>lt;sup>b</sup>Aylward and co-workers (44) report a diffusion coefficient of 7.7  $\pm$  0.3 x  $10^{-6}$  cm<sup>2</sup> sec<sup>-1</sup> for azobenzene.

that diffusion coefficients of Table VII depend on molecular weight. Thus, these data provide the interesting possibility of evaluating the Stokes-Einstein diffusion equation for calculating diffusion coefficients of molecular solutes. The Stokes-Einstein equation (13) is

$$D = \frac{RT}{A} \cdot \frac{1}{6\pi\eta r}$$

where  $\underline{D}$  is diffusion coefficient,  $\underline{n}$  viscosity coefficient of the solvent,  $\underline{r}$  radius of the molecule, and  $\underline{A}$  Avogadro's number. If the molecules are large spheres which do not polymerize or undergo appreciable solvation, and the molar volume in solution is the same as in the pure state, the radius can be calculated from the molecular weight,  $\underline{M} \cdot \underline{W} \cdot$ , and the density,  $\underline{d}$ , of the substance in the pure state by the relation

$$M.W. = \frac{4}{3} \pi r^3 Ad$$

Combination of these equations and evaluation of constant terms  $(T = 298^{\circ}K)$  results in

$$D = \frac{2.96 \times 10^{-7} (d)^{1/3}}{\eta (M.W.)^{1/3}} cm^{2} sec^{-1}$$

The dependence of <u>D</u> on  $(M.W.)^{-1/3}$  is illustrated in Figure 15. The slope of the line in Figure 15 has a value of  $4.9 \times 10^{-5}$ . However, based on a viscosity coefficient for pure DMF of 0.00802 dyne sec cm<sup>-2</sup> (51) and the assumption that density for the azobenzene compounds is 1.0, the theoretical slope is  $3.70 \times 10^{-5}$ . The assumption of unity

Figure 15. Variation of diffusion coefficient of substituted azobenzene compounds with molecular weight (error level,  $\pm$  0.2 x  $10^{-6}$  cm<sup>2</sup>sec<sup>-1</sup>).

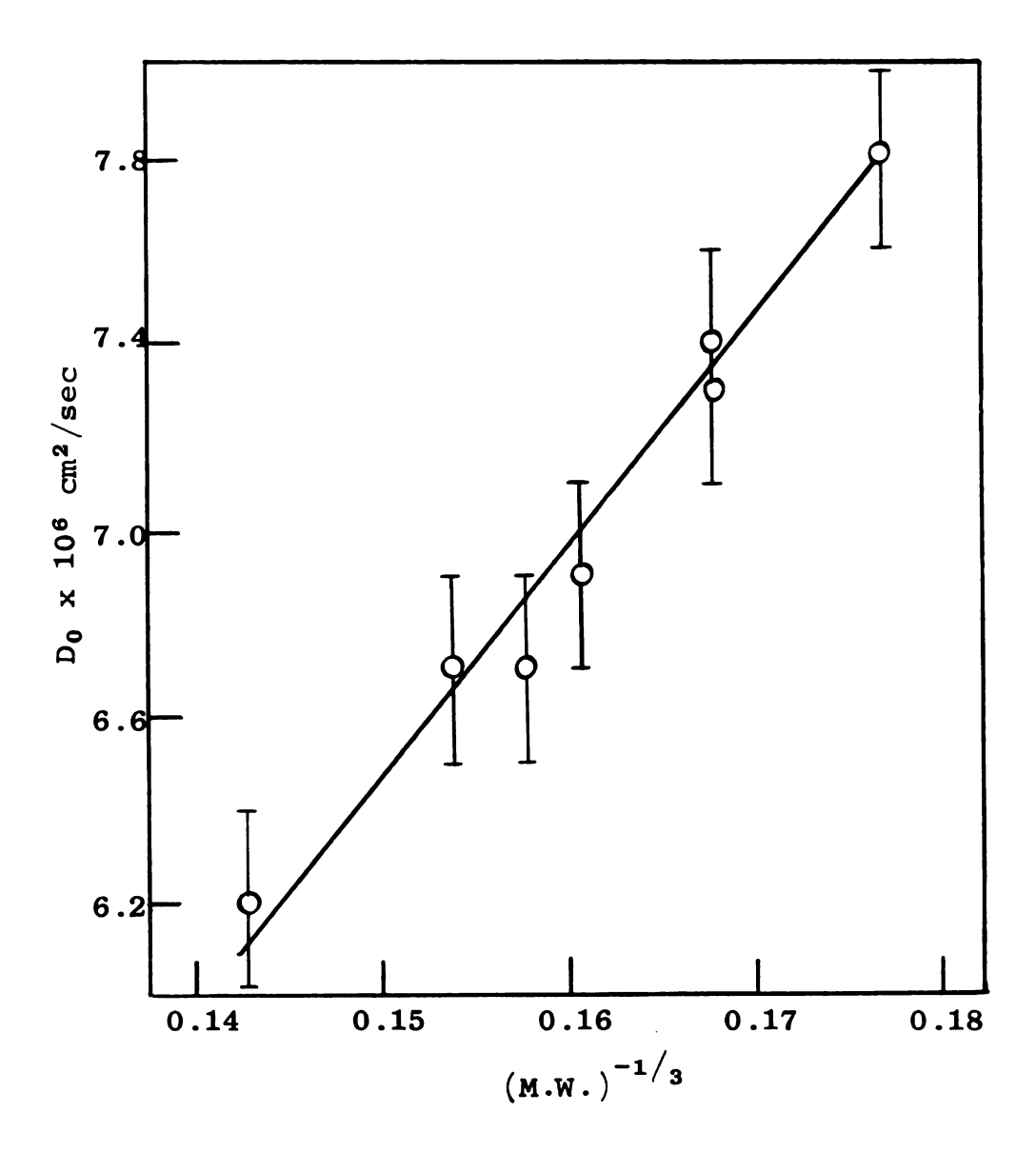


Figure 15

for density is reasonable because of the exponent (1/3) associated with density. Thus, errors in the theoretical slope resulting from inaccurate values of  $\underline{d}$  are at most about 6%. This error is smaller than the difference between theoretical and measured slopes. Experimental diffusion coefficients were determined in solutions containing  $0.3\underline{M}$  tetraethylammonium perchlorate. The Stokes-Einstein diffusion equation in the above form is only approximate (see above discussion) and generally applies at infinite dilution. These facts probably explain the discrepancy between theoretical and observed slopes.

# Effect of Double Layer Structure on Heterogeneous Rate Constants

The heterogeneous rate constants measured experimentally with cyclic voltammetry in the manner already discussed are apparent rate constants, because of the well-known influence of electrical double-layer structure on heterogeneous rate constants (52). Hence, for any of the conclusions made below between structure and reactivity to be meaningful, it is essential to evaluate effects of double-layer structure on the measured rate constants. Fortunately, for relative comparisons of the type discussed below, it is only necessary that double-layer corrections be constant for the series of rate constants. The discussion which follows demonstrates that these corrections are constant, and therefore no formal attempt to correct the apparent rate constants was made.

Electrical double-layer structure for tetraalkylammonium iodides at mercury-water interface has been investigated by Devanathan and Fernando (53). Their results for tetraethylammonium iodide indicate that the charge of the interface is relatively constant (15 to 17  $\mu$  coulombs cm<sup>-2</sup>) over the potential range considered in this investigation (-1.2 to -1.6 v versus SCE). Double-layer effects in DMF have been investigated by Minc and co-workers (54). Although they used lithium chloride and cesium iodide as supporting electrolyte, Frumkin (55) and Devanathan and Fernando (53) have shown that in water tetraalkylammonium iodide and cesium iodide cause very similar double-layer effects. At negative potentials anion contributions to double-layer structure are small because of repulsion from the electrode, and thus changing from iodide to perchlorate, which was used in this study, would result in only slight differences. Thus, by assuming that double-layer effects for tetraethylammonium idoide and cesium idoide are about the same in DMF, and applying Gouy-Chapman theory (applicability of this theory to non-aqueous solvents has been discussed by Grahame (56)) to evaluate these effects, the corrections which would be applied to apparent rate constants were found to be constant within about 5%, i.e.-within experimental error.

## Applicability of the Hammett Equation

If changes in free energies of several related equilibria are proportional to the change in some property of the substituents (such as electron withdrawing ability or resonance effects) a linear free-energy relationship results. Hammett has shown that a proportionality of this type describes the changes produced by meta and para substituents on equilibria involving phenyl-substituted compounds (57).

For benzene derivatives,  $X-C_6H_4-R$ , which have a polarographically active group, R, and substituent, X, in the meta or para position the Hammett equation for shifts in half wave potential with substituents (58) has the form

$$\Delta E_{1/2} = \rho \sigma$$

where  $\underline{\sigma}$  is the Hammett substituent constant (57). Values of substituent constants recently have been tabulated by Jaffe (59), and these values were used in comparisons below.  $\underline{\rho}$  is the reaction constant (expressed in volts) which reflects the sensitivity of the electrode process to the effects of substituents. It should be noted that the linear free energy relationship which is described by the above equation corresponds to free energy change for the overall electrode process i.e., free energy change between reactants and products.

An interesting fact about the generality of the Hammett equation is that it also has been used to correlate rates of reactions with substituent effects. This fact has made

possible the use of the Hammett equation in studying reaction mechanisms and effects of structure on reactivity. Thus, one might expect that the standard heterogeneous rate constants determined for a series of molecules of the type described above also would give a linear correlation with substituent constants. The equation relating  $\underline{k}_s$  and the free energy of activation,  $\Delta G^{\ddagger}$ , is

$$k_s = C \exp(-\Delta G^{\ddagger}/RT)$$

where  $\underline{C}$  is a constant and  $\underline{R}$  and  $\underline{T}$  have their usual meaning. Hence, a modified Hammett equation relating  $\underline{k}_{S}$  and  $\underline{\sigma}$  has the form

$$\log \frac{k_s}{k_{so}} = \rho \sigma$$

where  $\underline{k}_s$  and  $\underline{k}_{so}$  are the heterogeneous rate constants for the substituted and unsubstituted compounds respectively, and  $\underline{\sigma}$  and  $\underline{\rho}$  are defined above. Implicit in the derivation of this equation is the assumption that the reactants are in equilibrium with activated complex; therefore, if a linear free energy relation exists between  $\underline{k}_s$  and  $\underline{\sigma}$ , the free energy change between reactants and activated complex depends on substituents.

## Variation of Half-Wave Potentials with Structure

In Table VIII measured values of  $\underline{E_1}/_2$  for substituted azobenzene compounds are listed. These data are plotted versus the corresponding Hammett  $\underline{\sigma}$  values in Figure 16.

Table VIII.  $\underline{E_1}/_2$  and  $\underline{k}_s$  values for azobenzene compounds in N,N-dimethylformamide.

Compound .	$\frac{-\underline{E_1}/2}{2}$	$\frac{\underline{v},}{\text{volts}}$ $\underline{\text{sec}^{-1}}$	$\frac{n x \triangle \mathbf{E}}{p}$	Ψ	$\frac{k_{s}}{cm sec^{-1}}$
Azobenzene	1.420	29.1 43.5	77 79	1.41 1.25	0.25 0.25
1,1'-Azonaphthalene	1.200	30.0 42.3	80 84	1.19 0.99	0.18 0.18
4,4'-Dibromoazobenzene	1.256	30.0 42.3	70 73	2.40 1.85	0.35 0.34
4,4'-Dichloroazobenzene	1.265	30.0 42.3	70 72	2.40 2.00	0.37 0.37
4,4'-Diethylazobenzene	1.511	30.0 42.3	83 86	1.03 0.91	0.16 0.17
2,2'-Dimethylazobenzene	1.463	30.0 42.3	89 93	0.82 0.70	0.13 0.14
3,3'-Dimethylazobenzene	1.468	28.5 42.7	77 80	1.42 1.19	0.23 0.23
4,4'-Dimethylazobenzene	1.534	27.5 41.4	86 90	0.91 0.79	0.14 0.15

 $<sup>{}^{</sup>a}\underline{E}_{1/2}$  values  $\underline{\text{versus}}$  aqueous SCE, reproducibility  $\pm$  10 mv.

 $<sup>^{\</sup>rm b}\textsc{Error}$  level of  $\pm 10\%$  (see discussion in text).

Figure 16. Variation of  $\underline{E_1}_2$  with Hammett  $\underline{\sigma}$  value for substituted azobenzene compounds (slope, 0.36 volts;  $\underline{E_1}_2$   $\underline{vs}$  S.C.E.).

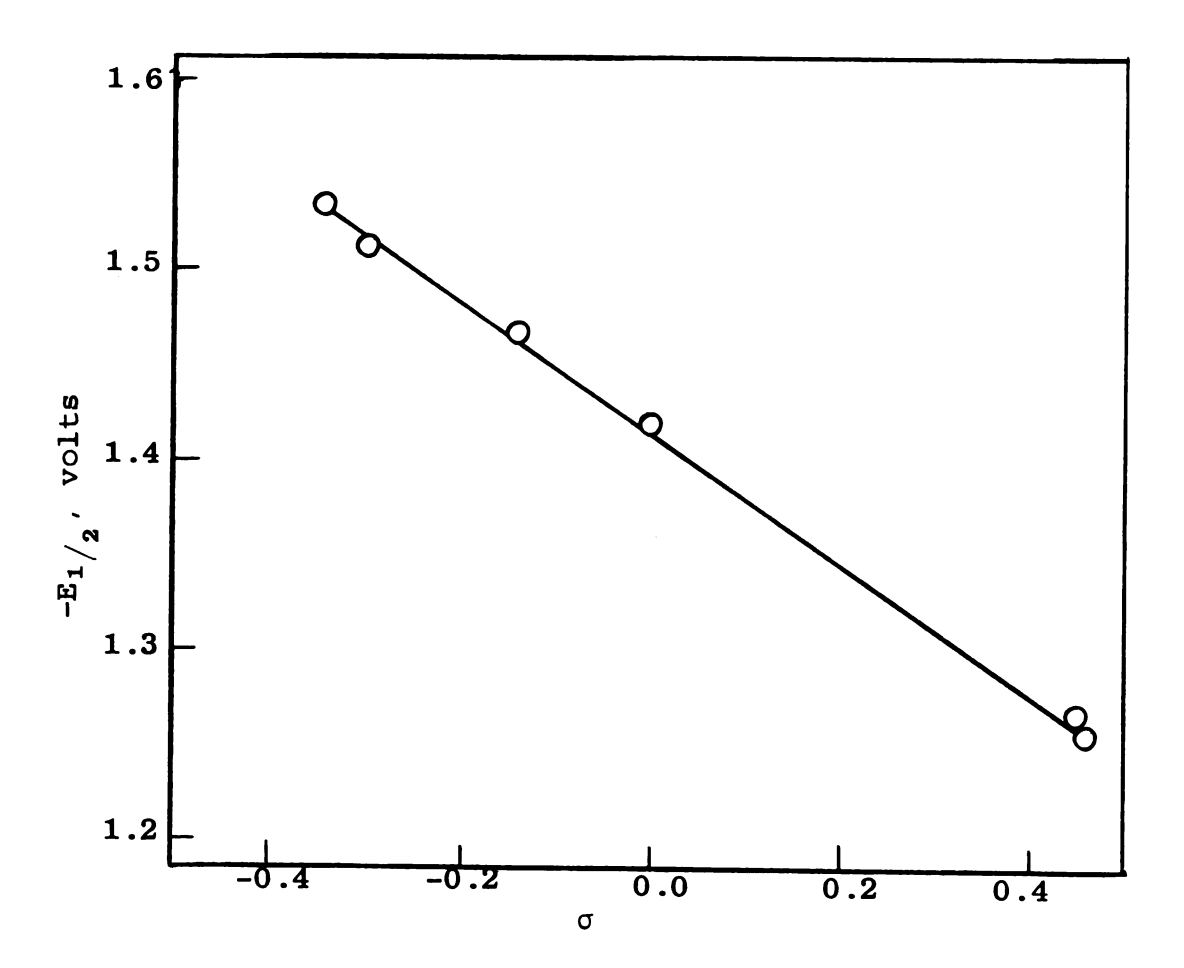


Figure 16

The points in Figure 16 define a straight line with slope (i.e., reaction constant,  $\rho$ ) of 0.36  $\pm$  0.01 volts. Substituted azobenzene compounds have been studied in aqueous solutions and correlations of this type also have been made (58). Values of  $\rho$  which were obtained in these correlations are considerably lower (0.08 at pH < 3.0 and 0.16 at pH =5-8) than the value obtained above. However, in aqueous solutions the reduction of azobenzene compounds follows a different mechanism than in DMF. The mechanism in aqueous solutions involves hydrogen ions and is not known in detail, therefore it may be that half-wave potentials are not directly related to free energy changes. For these reasons a direct comparison between the values of  $\rho$  reported here and those obtained by other workers is not possible. However, for polarographic studies of substituted nitrobenzene compounds in DMF with 0.1M tetraethylammonium iodide (60) a reaction constant of 0.42 was determined from correlations of half-wave potentials for the first reduction step (formation of nitrobenzene radical anion) with Hammett  $\sigma$  values. Because of the similarity of azobenzene and nitrobenzene compounds, and since the reduction mechanisms appear to be similar, the observed agreement between reaction constants for these series of compounds is reasonable.

## Variation of Heterogeneous Rate Constants with Structure

Measured values of  $\underline{k}_{\mathbf{S}}$  for azobenzene compounds are listed in Table VIII. These rate constants are accurate

within about  $\pm 10\%$ , even though measured rate constants show an average deviation of about  $\pm 3\%$  (6 runs), because of a combination of errors from  $\alpha$ ,  $\underline{D}_0$ , etc. Figure 17 is a plot of log  $\underline{k}_s$  versus Hammett  $\underline{\sigma}$  values (59) for substituted azobenzene compounds. The procedure described by Jaffe (59) was used to determine the slope,  $\underline{\rho}$ , which has a value of  $0.43 \pm 0.03$ .

An attempt to examine the effects of steric influences on measured values of  $\underline{E}_{1/2}$  and  $\underline{k}_{S}$  was made by investigating 2,2'-dimethylazobenzene (see Table VIII). Generally a given substituent operates with approximately equal strength from the ortho- and para- positions. Hence in the absence of steric effects one would expect that  $\underline{E}_{1/2}$  and  $\underline{k}_{S}$  for this compound would be nearly the same as for 4,4'-dimethyl-azobenzene. Experimentally, this appears to be the case, because  $\underline{E}_{1/2}$  values for these two compounds differ by only about 70 mv, and  $\underline{k}_{S}$  for 2,2'-dimethylazobenzene is about the same as for 4,4'-dimethylazobenzene (0.13 and 0.15 cm sec<sup>-1</sup> respectively). Although sufficient data are not available, the implication of these results is that steric effects do not play a major role in determining the activation energy for these electrode reactions.

The data for 1,1'-azonaphthalene (see Table VIII) clearly cannot be used in above comparisons. However, it appears that a study of reactivity versus structure could be made with a series of substituted azonaphthalene compounds, because the mechanism for reduction is analogous to that of azobenzene.

Figure 17. Variation of  $\underline{k}_s$  with Hammett  $\underline{\sigma}$  value for substituted azobenzene compounds (slope, 0.43  $\pm$  0.03; error level,  $\pm$  10%).

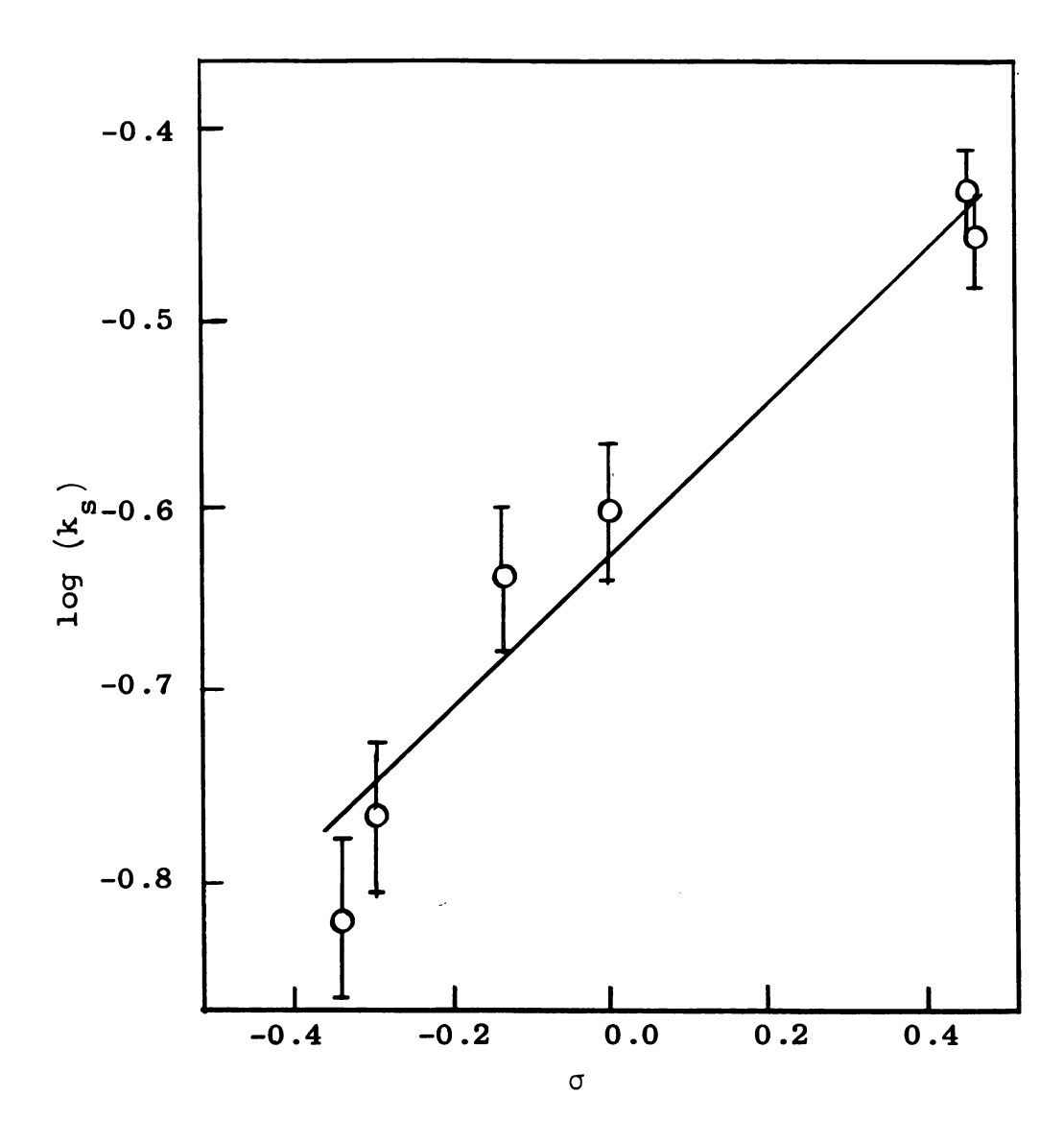


Figure 17

A literature survey indicates that this is the first time linear free energy correlations with heterogeneous rate constants have been cited, and therefore these results are important for several reasons. For example, they imply that it may be possible to estimate values of  $\underline{k}_s$  for aromatic compounds whose Hammett sigma values are known, and  $\underline{k}_s$  for the parent compound has been measured. In addition, the results illustrate the type of structural changes that produce large values of  $\underline{k}_s$ , something that is of considerable practical importance. Finally, they indicate that more detailed studies of the above type may provide valuable information about the structure of activated complex during electron transfer, by, for example, comparing measured free energies of activation with quantum mechanical calculations for different configurations of the activated complex.

## MECHANISM OF REDUCTION OF AZOBENZENE IN WATER

Reduction of azobenzene in protic solvents is a two electron process involving two hydrogen ions. Polarographic experiments have shown that the apparent reversibility of the electron transfer depends on hydrogen ion concentration, the electrode process becoming less reversible as pH is raised (23-33). To account for these facts some workers have suggested a stepwise reduction with a single hydrogen ion involved in each step (24), but no experimental data have been presented to prove or refute this idea. Thus, the possibility exists that in aqueous solvents the reduction may involve two electrons with 0, 1, or 2 hydrogen ions in the rate determining step with the remaining hydrogen ions participating in preceding and or succeeding equilibria.

In an effort to resolve these possibilities cyclic voltammetry was used to measure apparent heterogeneous rate constants for reduction of azobenzene, and the dependence of these rate constants on pH was determined. Because available theory of cyclic voltammetry could not be applied directly to reactions involving hydrogen ion, it also was necessary to extend the theory to include these cases. Results of this theory together with applications to kinetics of azobenzene reduction constitute the final part of this thesis.

#### THEORY

Theory of cyclic voltammetry for the mechanism

$$0 + ne \xrightarrow{\frac{k}{f}} R$$

is given by Nicholson (14). For this simple case theory takes the form of the following integral equation

$$\frac{\chi(y) \left(\gamma \theta s_{\lambda}(y)\right)^{\alpha}}{\psi} = 1 - \int_{0}^{y} \frac{\chi(z)dz}{\sqrt{y-z}} - s_{\lambda}(y) - \gamma \theta s_{\lambda}(y) \int_{0}^{y} \frac{\chi(z)dz}{\sqrt{y-z}} (32)$$

where

$$\chi(\dot{\mathbf{y}}) = \frac{\mathbf{i}}{\mathrm{nFAC_O^*} \sqrt{\pi \mathrm{aD_0}}}$$
 (33)

$$y = at$$
 (34)

$$\gamma = \left(\frac{D_0}{D_R}\right)^{1/2} \tag{35}$$

$$\psi = \gamma^{\alpha} k_{s} / \sqrt{\pi a D_{0}}$$
 (36)

$$\gamma \theta = \exp \left(\frac{nF}{RT}\right) \left(E_{i} - E_{1/2}\right) \tag{37}$$

There  $\underline{\alpha}$  is the transfer coefficient and  $\underline{k}_s$  the standard heterogeneous rate constant at  $\underline{E}$  =  $E_1/_2$ . The function  $S_{\lambda}(y)$  is defined as

$$s_{\lambda}(y) = \begin{cases} \exp(-y) & \text{t } < \lambda \\ \exp(-y - 2a\lambda) & \text{t } > \lambda \end{cases}$$
(38)

where  $\underline{\lambda}$  is the switching time.

Numerical solutions of Equation 32 are presented in the form of a working curve that relates peak potential separations,  $\Delta \underline{\mathbf{E}}_p$ , to the kinetic parameter,  $\underline{\psi}$  (details of this working curve already were discussed in the section dealing with measurement of  $\underline{\mathbf{k}}_s$  values in DMF).

The above theory clearly applies only to compounds that are reduced according to Mechanism II. For reduction of azobenzene the following more general mechanism must be considered

$$A + mH^{+} \xrightarrow{K_{1}} O + ne + pH^{+} \xrightarrow{k_{f}} R + qH^{+} \xrightarrow{K_{2}} Z$$
 III

There  $\underline{K}_1$  and  $\underline{K}_2$  are equilibrium constants for possible preceding and succeeding reactions,  $\underline{k}_f$  and  $\underline{k}_b$  are heterogeneous rate constants of the electron transfer, 0 and R represent oxidized and reduced forms of depolarizer, and A and Z are electroinactive.

Mechanism III is very difficult because the partial differential equations would be nonlinear. However, if hydrogen ion concentration is large with respect to depolarizer concentration, then reactions involving hydrogen ion can be treated as pseudo-first order, and the differential equations will be linear. Under these conditions Mechanism III can be treated by following exactly the procedure outlined by Nicholson (14) for Mechanism III. In this case the following integral equation results

$$\frac{\chi(y)(\gamma\theta s_{\lambda}'(y))^{\alpha}}{\psi^{\dagger}} = 1 - \int_{0}^{y} \frac{\chi(z)dz}{\sqrt{y-z}} - s_{\lambda}(y) - \theta s_{\lambda}'(y) \int_{0}^{y} \frac{\chi(z)dz}{\sqrt{y-z}}$$
(39)

where

$$\theta = \frac{C_A^*}{C_Z^*} \tag{40}$$

$$S_{\lambda}'(y) = S_{\lambda}(y) \exp(\frac{RT}{nF}) \ln[H^{+}]^{m+q} K_{1}K_{2}$$
 (41)

$$\psi' = \psi[H^+]^{p(1-\alpha)}$$
 (42)

and other terms retain the definitions given in connection with Equation 32.

Several limiting cases of Mechanism III follow directly from Equation 39. For example, when there is no succeeding equilibrium

$$\theta = \frac{C_{A}^{*}}{C_{R}^{*}} \tag{43}$$

and

$$S_{\lambda}'(y) = S_{\lambda}(y) \exp(\frac{RT}{nF}) \ln[H^{+}]^{m} K_{1}$$
 (44)

Interestingly Equation 39 is formally identical with Equation 32. The important consequence of this fact is that solutions of Equation 32 also are solutions of Equation 39. Thus, solutions of Equation 39 will be exactly the same as those for Equation 32 except that the calculated anodic and cathodic currents will be displaced by a constant value along the potential axis depending on the value of  $\underline{K}_1$   $\underline{K}_2$   $[\underline{H}^+]^{m+q}$ . The value of  $\underline{n}$  x  $\Delta \underline{E}_p$  will be independent of  $\underline{K}_1$   $\underline{K}_2$   $[\underline{H}^+]^{m+q}$  since the quantity  $\exp\{(\frac{RT}{nF})\ln[\underline{H}^+]^{m+q}K_1k_2\}$ 

appears both in the anodic and cathodic potential functions. Thus, values of  $\underline{\psi}$ ' can be obtained directly from the working curve developed by Nicholson (14) without the necessity of additional numerical calculations. From these values of  $\underline{\psi}$ ', a value of the apparent heterogeneous rate constant,  $\left(\underline{k}_{s}\right)_{app}$  is obtained. From the definition of  $\underline{\psi}$  and  $\underline{\psi}$ ', this value of  $\left(\underline{k}_{s}\right)_{app}$  equals  $\underline{k}_{s}[\mathtt{H}^{+}]^{p(1-\alpha)}$ , where  $\underline{k}_{s}$  is the true rate constant. Hence if  $\underline{\alpha}$  is known the number of hydrogen ions in the rate determining step  $(\underline{p})$  is readily obtained from a plot of  $(\underline{k}_{s})_{app}$  versus hydrogen ion concentration.

### EXPERIMENTAL

Instrumentation and experimental procedures were identical with those discussed in connection with applications of the potential step-linear scan method, except the detector was an x-y recorder. Also, for solutions of azobenzene in 50 wt % ethanol-water, enough lithium perchlorate was added to maintain ionic strength at  $0.75\underline{\text{M}}$ .

## RESULTS AND DISCUSSION

For all experiments the concentration of perchloric acid was low enough that the extent of benzidine rearrangement was negligible, and therefore had no effect on current-voltage curves. Also, by using relatively low acid concentrations adsorption of azobenzene and hydrazobenzene was considerably reduced. Finally, to comply with the theoretical model concentration of azobenzene always was at least an order of magnitude smaller than the acid concentration.

Measured values of  $\underline{E_1}/_2$  versus SCE and the apparent standard rate constant,  $(\underline{k}_s)_{app}$ , at various acid concentrations are listed in Table IX. Figure 18 is a plot of  $\underline{E_1}/_2$  versus -log [H<sup>+</sup>]; the straight line has a slope of 56 mv consistent with two hydrogen ions participating in the overall electrode reaction.

If the electrode reaction is consistent with the theory described above then a plot of log  $(\underline{k}_s)_{app}$  versus log  $[H^{\dagger}]$  should be a straight line of slope  $\underline{p}(1-\alpha)$  (see Figure 19). The straight line that has been drawn in Figure 19 has a slope of 0.76. Thus, if  $\underline{p}=1$ ,  $\underline{\alpha}=0.24$ , and if  $\underline{p}=2$ ,  $\underline{\alpha}=0.62$ . Also a plot of  $[H^{\dagger}]^{0.76}$  versus  $(\underline{k}_s)_{app}$  is a straight line (see Figure 20) with intercept of 0.0, and slope equal to the true value of  $\underline{k}_s$ , which was found to be 0.105 cm/sec.

These above results are consistent with three limiting mechanisms of the general Mechanism III where either one or

Table IX. Variation of  $\underline{E_1}_2$  and  $(\underline{k}_s)_{app}$  with hydrogen ion concentration for reduction of azobenzene in aqueous solutions.

[H <sup>+</sup> ], <u>M</u>	$\frac{E_1}{2}$ , volts	v,mv/sec	$\underline{\underline{n}} \times \Delta \underline{\underline{E}}_{p}, \underline{m} v$	ψ '	$(\underline{k}_s)_{app}^{c} \times 10^3$
0.500	0.024	100 140	63.2 64.0	6.70 6.00	<b>61</b> 65
0.100	-0.013	106 177	72.0 76.0	2.00 1.50	19 18
0.050	-0.029	70.8 106	76.0 80.0	1.50 1.20	12 11
0.010	-0.071	35.4 70.8	106 116	0.49 0.38	2.8 2.9

 $<sup>^{</sup>a}$ Concentration of azobenzene was 1mM.

 $b_{\underline{E}_1/2}$  values <u>versus</u> SCE.

<sup>&</sup>lt;sup>C</sup>Each value of  $\left(\underline{k}_{s}\right)_{app}$  listed is average of 3 experiments.

Figure 18. Variation of  $\underline{E_1}/_2$  with perchloric acid concentration for reduction of azobenzene (slope, 56 mv per unit pH change;  $\underline{E_1}/_2$   $\underline{\text{vs}}$  S.C.E.).

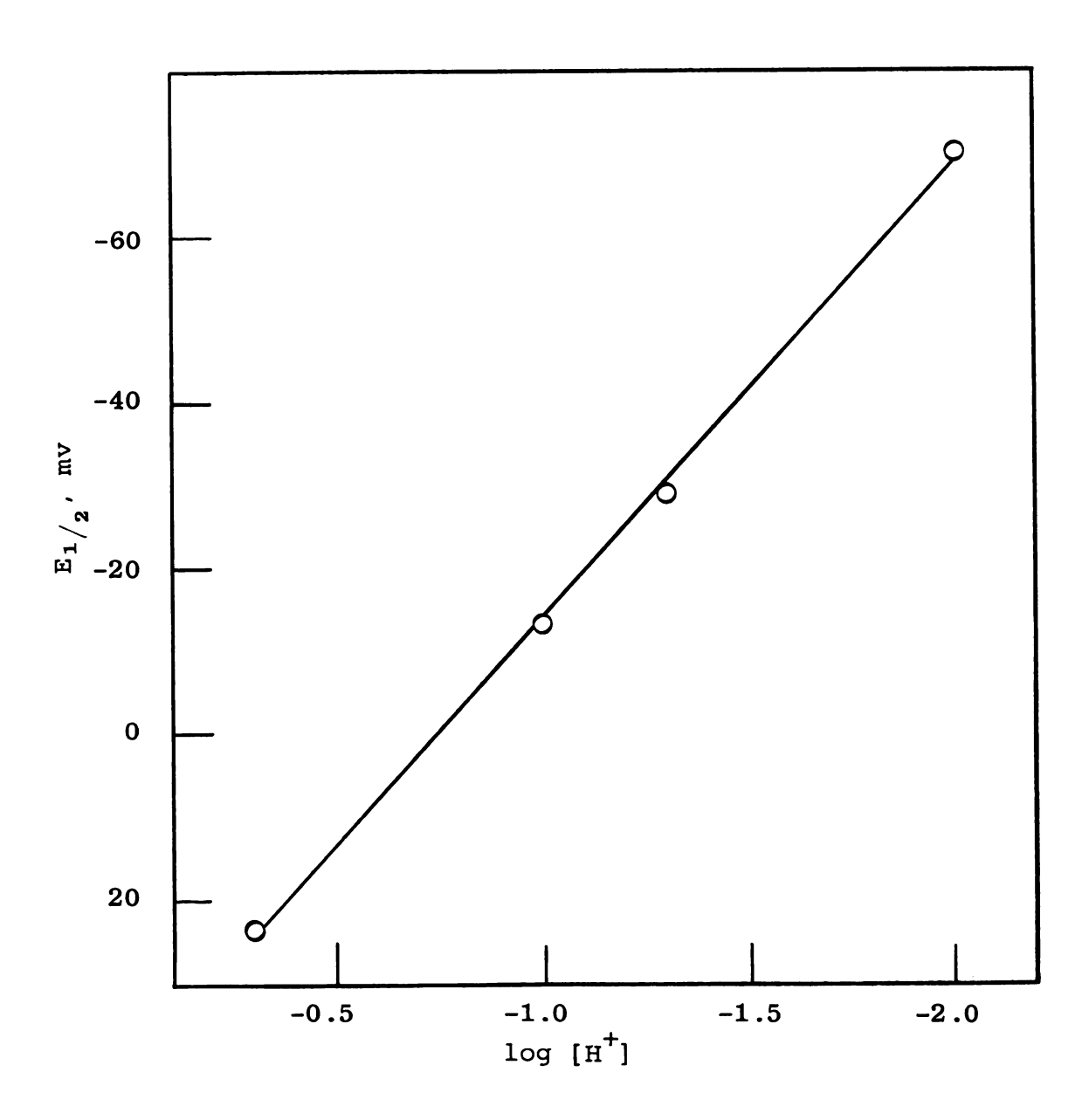


Figure 18

Figure 19. Variation of  $\left(\underline{k}_s\right)_{app}$  with perchloric acid concentration for reduction of azobenzene (slope, 0.76).

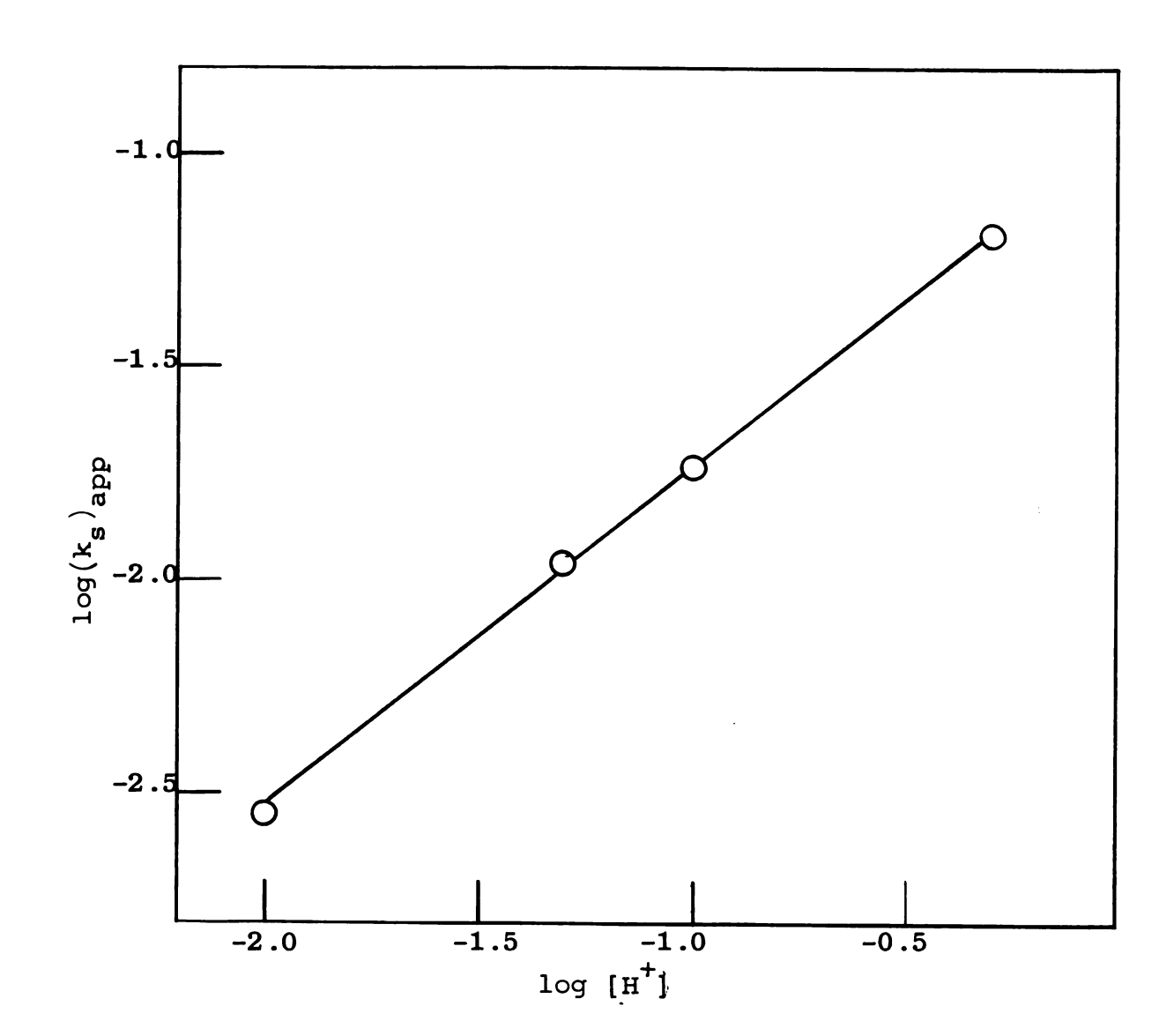


Figure 19

Figure 20. Variation of  $(\underline{k}_s)_{app}$  with  $[H^+]^{0.76}$  for reduction of azobenzene (slope, 0.105 cm sec<sup>-1</sup>).

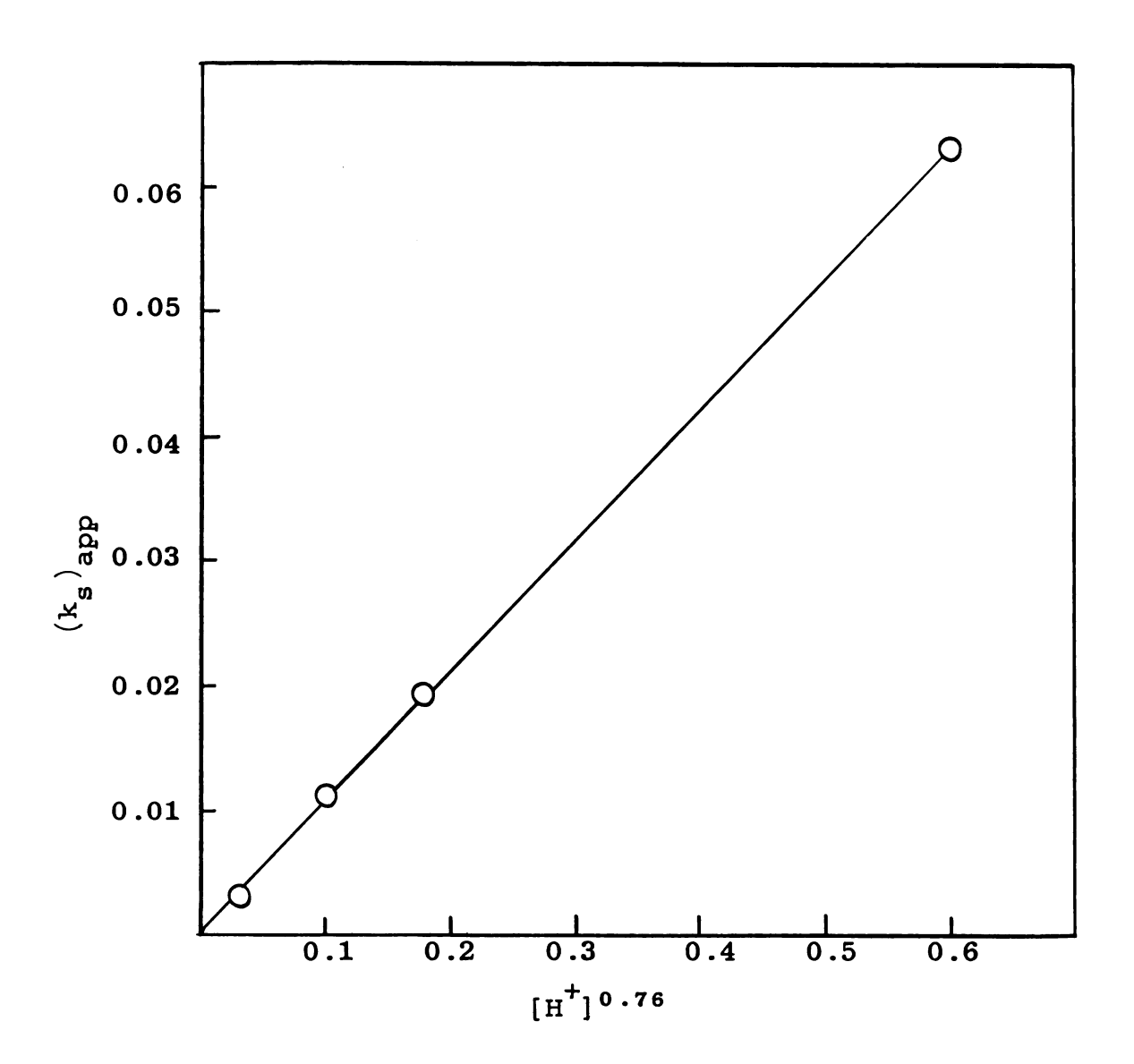


Figure 20

two hydrogen ions are involved in the rate determining step:

$$A + H^{+} \xrightarrow{K} O + 2e + H^{+} \xrightarrow{k_{f}} R$$
 IV

$$A + 2e + H^{+} \xrightarrow{k_{f}} R' + H^{+} \xrightarrow{K} R$$

$$A + 2e + 2H^{+} \xrightarrow{k_{f}} R$$
 VI

There  $\underline{A}$  represents azobenzene,  $\underline{O}$  is protonated azobenzene,  $\underline{R}$ ' is the anion of hydrazobenzene, and  $\underline{R}$  is hydrazobenzene.

To reduce further the number of possible mechanisms the value of  $\underline{\alpha}$  must be known. An approximate value of  $\underline{\alpha}$  can be obtained from experimental current-voltage curves by a comparison with theoretical curves calculated for several values of  $\underline{\alpha}$  and a given value of  $\underline{\psi}$ . This comparison is illustrated in Figure 21 for  $\underline{\psi}=2.00$  (determined from peak potential separation  $\underline{n} \times \Delta \underline{E}_{\underline{p}} = 72 mv$ ). The best agreement between theory and experiment is obtained for  $\underline{\alpha}$  equal about 0.7, which indicates that  $\underline{p}$  for the system is 2. Therefore, these data strongly suggest that both hydrogen ions are involved directly with the electron transfer reactions, not in preceding or succeeding chemical equilibria --i.e. Mechanism VI above.

The above data do not, however, distinguish between a concerted two-electron transfer and two stepwise one-electron additions each involving a single proton. Because a concerted two-electron reduction is unlikely, the latter

Figure 21. Comparison of theory and experiment.

- o, theory  $(\underline{\alpha}, 0.7; \underline{\psi}, 2.0)$
- $\square$ , theory ( $\underline{\alpha}$ , 0.5;  $\underline{\psi}$ , 2.0)
- $\triangle$ , theory ( $\underline{\alpha}$ , 0.3;  $\underline{\psi}$ , 2.0)
- ---, experiment for reduction of  $\underline{\text{mM}}$  azobenzene in  $0.1\underline{\text{M}}$  perchloric acid (scan rate, 106 mv sec  $\underline{\text{E}_1}_{/2}$ ,  $\overline{0.013}$  v vs S.C.E.).

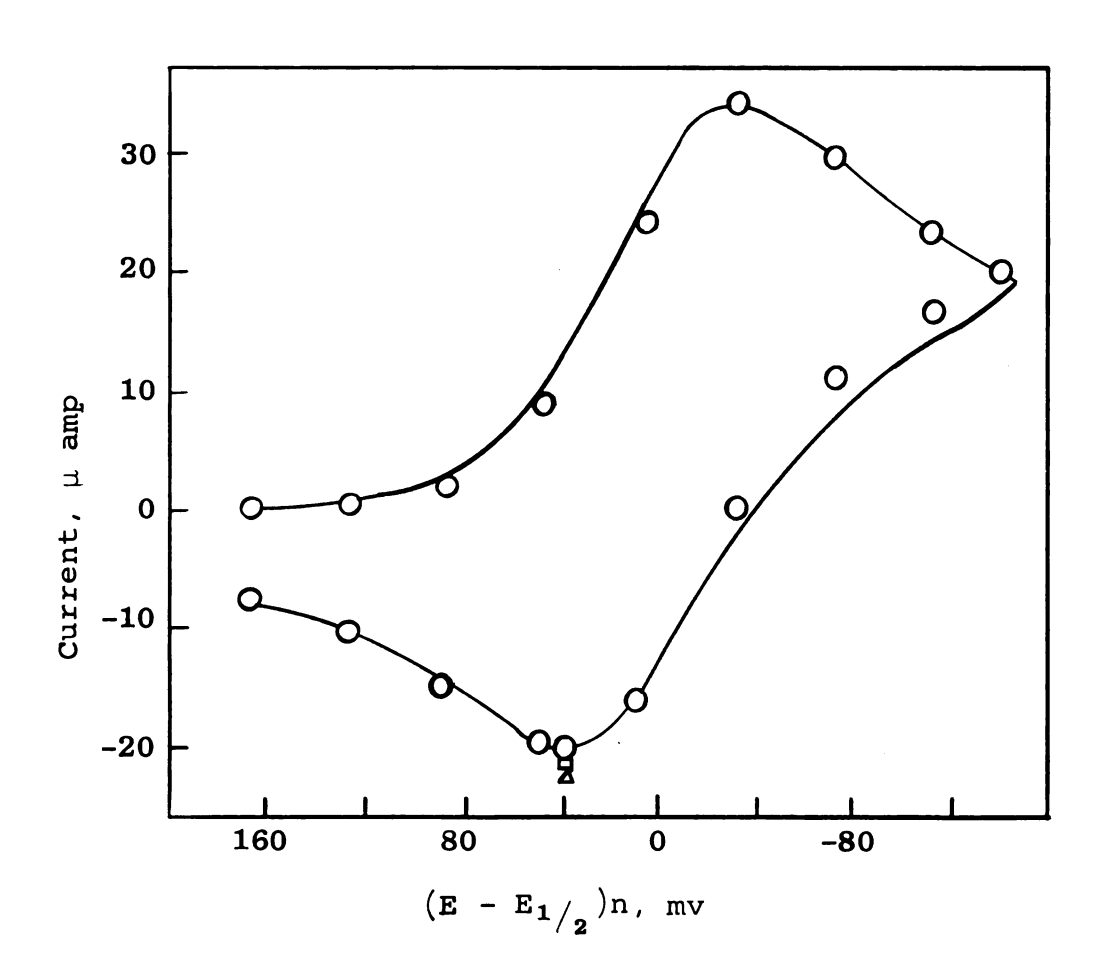


Figure 21

mechanism seems most probable; in fact experiments in DMF to which various amounts of a proton donor have been added suggest stepwise reduction. Typical results of such experiments are shown in Figure 22. In Figure 22, curve A corresponds to reduction of azobenzene (given the symbol A in following mechanisms) in DMF with no added proton donor. These curves were discussed earlier where it was shown that Wave I results from formation of the monoanion of azobenzene

$$A + e \longrightarrow A$$
 VII

and Wave II corresponds to formation of the dianion

$$A^- + e \longrightarrow A^-$$
 VIII

and Wave III is the reverse of Reaction VII.

On addition of benzoic acid curve B of Figure 22 results. Thus, the effect of proton donor is to increase the height of Wave I, with a corresponding decrease in Waves II and III. Also, a new wave, Wave IV, appears at more anodic potentials. These results can be explained by postulating that Wave I now results from the following parallel reactions

$$A + e \longrightarrow A$$
 IX

$$A + e + H^{+} \longrightarrow AH$$
 X

Because  $\underline{AH}$  should be more easily reduced than  $\underline{A}$  (64), any  $\underline{AH}$  that is formed (the amount will depend on the effective acid concentration) is reduced immediately

$$AH + e + H^{+} \longrightarrow AH_{2}$$
 XI

Figure 22.

Cyclic stationary electrode polarograms for reduction of 0.4mM azobenzene in 0.3M tetraethylammonium perchlorate and N.N-dimethylformamide with varying amounts of benzoic acid (scan rate, 40 v sec<sup>-1</sup>).

D, C, D,

no benzoic acid

1mM benzoic acid
10mM benzoic acid
10mM benzoic acid, 50% by volume,

N.N-dimethylformamide-water

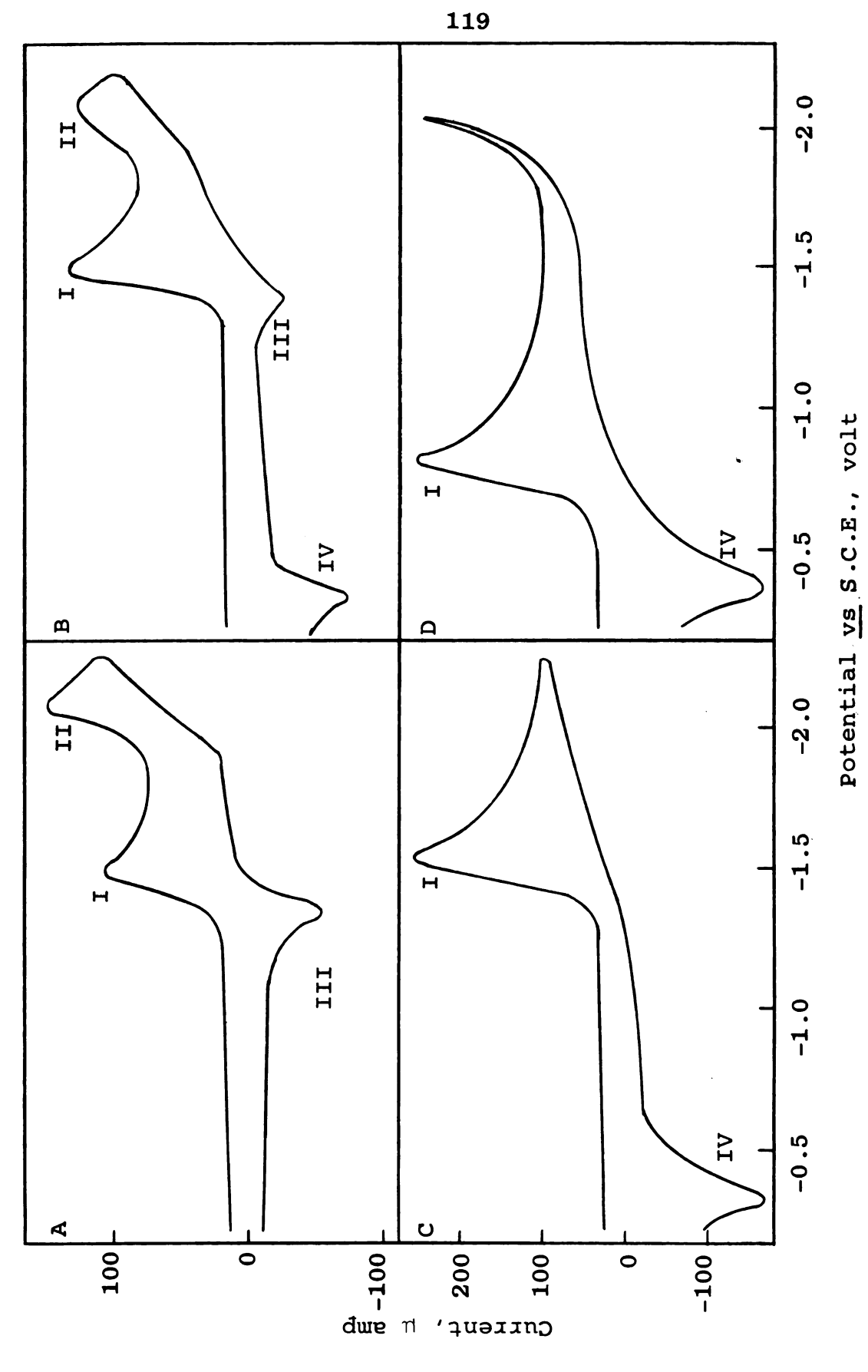


Figure 22

causing an increase in the height of Wave I. The decrease of Waves II and III follows directly because now less A is present for reduction at Wave II, and oxidation at Wave III. Also, Wave IV is explained by assuming that it represents oxidation of the AH<sub>2</sub> formed during Wave I by the reverse of Reactions X and XI.

On further addition of benzoic acid curve C of Figure 22 is obtained. This curve is consistent with the reactions already postulated where now there is sufficient proton concentration that for Wave I the second of the parallel reactions (Reaction X) predominates. Thus, Wave I results from Reactions X and XI, where Reaction X is rate determining because of the difference of reduction potentials discussed above for Reactions X and XI. Again, Wave IV corresponds to the reverse of Reactions X and XI.

On addition of more benzoic acid no significant changes occur, probably because benzoic acid in DMF is a weak enough acid that further increases in its concentration do not increase proton concentration (65). These ideas are substantiated by the fact that on addition of water curve D of Figure 22 results (also, curves essentially identical with A, B, C, and D of Figure 22 are obtained by using sulfuric acid as proton donor, in which case curve D results without the addition of water). If this explanation is correct the postulated reactions readily explain the transition from curve C to curve D. Thus, as proton concentration increases the rate of Reaction X increases, and

an anodic shift for Wave I results (see curve D). Because the rate of the reverse of Reactions X and XI is independent of hydrogen ion concentration, the potential of Wave IV does not shift until the whole process becomes reversible—that is  $\Delta \underline{E}_p$  between Waves I and IV is 30 mv. Beyond this point the electrode reaction is perfectly reversible, both Waves I and IV shifting 60 mv per unit change of pH, as already discussed (Figure 18).

Although the above discussion is only qualitative, the proposed step-wise mechanism is consistent with two hydrogen ions ( $\underline{p} = 2$ ) involved in the electrode reaction. In addition, it appears to explain the transition from non-aqueous to aqueous experimental results. However, to prove this mechanism would require extensive additional theoretical calculations and experimental data.

#### LITERATURE CITED

- 1. Kern, D. M. H., J. Am. Chem. Soc., <u>75</u>, 2473 (1953); <u>76</u>, 1011(1954).
- Konrad D. and A. A. Vlcek, Collection Czech. Chem. Commun., 28, 808 (1963).
- 3. Kivalo, P., Acta Chem. Scand., 9, 221 (1955).
- 4. Koutecky, J., Collection Czech. Chem. Commun., 20, 116 (1955).
- Testa, A. C. and W. H. Reinmuth, Anal. Chem., <u>32</u>, 1512 (1960).
- 6. Dracka, O., Collection Czech. Chem. Commun., 25, 338 (1960).
- 7. Jaenicke, W. and H. Hoffmann, Z. Electrochem., <u>66</u>, 803, 814 (1962).
- 8. Herman, H. B. and A. J. Bard, Anal. Chem., 36, 510 (1964).
- 9. Schwarz, W. M. and I. Shain, J. Phys. Chem., 69, 30 (1965).
- 10. Nicholson, R. S. and I. Shain, Anal. Chem., 36, 706 (1964).
- 11. Schwarz, W. M. and I. Shain, J. Phys. Chem., <u>70</u>, 845 (1966).
- 12. Reinmuth, W. H., Anal. Chem., 34, 1446 (1962).
- 13. Kolthoff, I. M. and J. J. Lingane, "Polarography", Interscience Publishers, New York, N.Y., 1952, Chapter II, III.
- 14. Nicholson, R. S., Anal. Chem., <u>37</u>, 1351 (1965).
- 15. Churchill, R. V., "Operational Mathematics", McGraw-Hill Book Co., Inc., New York, N.Y., 1958, Chapter II.
- 16. Irving, J. and N. Mullineux, "Mathematics in Physics and Engineering", Academic Press Inc., New York, N.Y., 1959, Chapter XII and Appendix.
- 17. <u>Ibid.</u>, Chapter X.
- 18. Cottrell, F. G., Z. Physik. Chem., 42, 385 (1902).

- 19. Olmstead, M. L. and R. S. Nicholson, J. Electroanal. Chem., in press.
- 20. Huber, A., Monatsh. Mathematik und Physik, <u>47</u>, 5323 (1939).
- 21. Reinmuth, W. H., J. Am. Chem. Soc., 79, 6358 (1957).
- 22. Martin, K. and I. Shain, J. Phys. Chem., 65, 254 (1961).
- 23. Foffani, A. and M. Fragiacomo, Ric. Sci., 22, 139 (1952).
- 24. Hillson, P. J. and P. P. Birnbaum, Trans. Faraday Soc., 48, 478 (1952).
- 25. Castor, C. R. and J. H. Saylor, J. Am. Chem. Soc., <u>75</u>, 1427 (1953).
- 26. Wawzonek, S. and J. D. Fredrickson, J. Am. Chem. Soc., 77, 3985, 3988 (1955).
- 27. Nygard, B., Arkiv. Kemi, 20, 163 (1963).
- 28. Markman, A. L. and E. V. Zinkova, J. Gen. Chem. U.S.S.R., 29, 3058 (1959).
- 29. Florence, T. M. and Y. J. Farrar, Australian J. Chem., 17, 1085 (1964).
- 30. Holleck, L. and G. Holleck, Naturwissenschaften, 51, 212, 433 (1964).
- 31. Holleck, L., A. M. Shams-El-Din, R. M. Saleh and G. Holleck, Z. Naturforsch., 19, 161 (1964).
- 32. Holleck, L. and G. Holleck, Monatsh. Chem., <u>95</u>, 990 (1964).
- 33. Chuang, L., I. Fried and P. J. Elving, Anal. Chem., 37, 1528 (1965).
- 34. Banthorpe, D. V., E. D. Hughes and C. K. Ingold, J. Chem. Soc., 2864 (1964), and references therein.
- 35. Oglesby, D. M., J. D. Johnson and C. N. Reilley, Anal. Chem., 38, 385 (1966).
- 36. Carlin, R. B. and R. C. Odioso, J. Am. Chem. Soc., 76, 2345 (1954).
- 37. Wopschall, R. H. and I. Shain, Anal. Chem., 39, 1514, 1527, 1535 (1967).

- 38. Nicholson, R. S., Anal. Chem., 37, 667 (1965).
- 39. Schwarz, W. M. and I. Shain, Anal. Chem., <u>35</u>, 1770 (1963).
- 40. Ross, J. W., R. D. DeMars and I. Shain, Anal. Chem., 28, 1768 (1956).
- 41. Schultz, G., Ber., 17, 473 (1884).
- 42. Croce, L. J. and J. D. Gettler, J. Am. Chem. Soc., 75, 874 (1953).
- 43. Wawzonek, S. and A. Gundersen, J. Electrochem. Soc., 111, 324 (1964), and references therein.
- 44. Aylward, G. H., J. L. Garnett, and J. H. Sharp, Anal. Chem., 39, 457 (1967).
- 45. Thomas, A. B. and E. G. Rochow, J. Am. Chem. Soc., 79, 1843 (1957).
- 46. Brown, H. C. and W. H. Bonner, J. Am. Chem. Soc., <u>76</u>, 605 (1954).
- 47. Raman, P. S., Proc. Indian Acad. Sci., 45, 65 (1957).
- 48. Santurri, P., F. Robbins, and R. Stubbings, Organic Synthesis, 40, 18 (1960).
- 49. Kolthoff, I. M. and J. F. Coetzee, J. Am. Chem. Soc., 79, 870 (1957).
- 50. Booman, G. L. and W. B. Holbrook, Anal. Chem., <u>37</u>, 795 (1965).
- 51. Meek, D. W. "The Chemistry of Nonaqueous Solvents", J. J. Lagowski, Ed., Academic Press, New York, N.Y., 1966, p. 57.
- 52. Delahay, P., "Double Layer and Electrode Kinetics", Interscience Publishers, New York, N. Y., 1965.
- 53. Devanthan, M. A. V. and M. J. Fernando, Trans. Faraday Soc., 58, 368 (1962).
- 54. Minc, S., J. Jastrzebska, and M. Brzostowska, J. Electrochem. Soc., 108, 1160 (1961).
- 55. Frumkin, A. N., B. B. Damaskin, and N. Nikolaeva-Fedorovich, Doklady Akad. Nauk S.S.S.R., 115, 751 (1957).
- 56. Grahame, D. C., Z. Electrochem., 59, 740 (1955).

- 57. Hammett, L. P., Chem. Rev., 17, 125 (1935).
- 58. Zuman, P., Collection Czech. Chem. Commun., 25, 3225 (1960).
- 59. Jaffe, H. H., Chem. Rev., 53, 191 (1953).
- 60. Holleck, L. and D. Becher, J. Electroanal. Chem.,  $\underline{4}$ , 321 (1962).
- 61. Newbold, B. T. and D. Tong, Canadian J. Chem., <u>42</u>, 836 (1964).
- 62. Hoogewerff, S. and W. A. vanDorp, Ber., 11, 1203 (1878).
- 63. Nolting, E. and T. Stricker, Ber., 21, 3139 (1888).
- 64. Hoijtink, G. J., J. vanSchooten, E. deBoer, and W. Albersberg, Rec. Trav. Chim., 73, 355 (1954).
- 65. Price, E., "The Chemistry of Nonaqueous Solvents,"
  J. J. Lagowski, Ed., Academic Press, New York, N.Y.,
  1966, p. 92.

## APPENDIX A

# Numerical Solution of Equation 22 for the Potential Step Linear Scan Method

The method of Huber (20) was used to evaluate numerically  $\chi(\underline{z})$  in Equation 22 of the text. The method approximates the function  $\chi(\underline{z})$  by a straight line of slope  $\underline{\alpha}$  on a given interval of width  $\underline{\delta}$  along the  $\underline{z}$  axis. Evaluation of  $\underline{\alpha}$  defines the function  $\chi(\underline{at})$  on each interval. Thus,  $\chi(\underline{at})$  on any interval,  $\underline{i}$ , is equal to  $\underline{\delta}$  times the sum of all previous  $\underline{\alpha}$ 

$$\chi(at) = \delta \sum_{k=1}^{i} \alpha_{k}$$
 (<sub>1A</sub>)

Equation 22 can be reduced to a recursion formula to calculate the individual values of  $\underline{\alpha}$  (20)

$$\alpha_{\mathbf{k}} = \frac{1.00 - \sum_{\mathbf{i}=1}^{\mathbf{k}-1} \alpha_{\mathbf{i}} [\mathbf{A}_{\mathbf{k}-\mathbf{i}+1}] - \mathbf{S}(\mathbf{k}\delta) \sum_{\mathbf{i}=1}^{\mathbf{k}-1} \alpha_{\mathbf{i}} [\mathbf{B}_{\mathbf{k}-\mathbf{i}+1}]}{[\delta \phi_{\mathbf{i}} - \psi_{\mathbf{i}}] + \mathbf{S}(\mathbf{k}\delta) [\delta \phi_{\mathbf{i}}^{\dagger} - \psi_{\mathbf{i}}^{\dagger}]}$$
(2A)

where

$$A_{j} = [\delta j] \{ \phi_{j} - \phi_{j-1} \} + \delta \phi_{j-1} - [\psi_{j} - \psi_{j-1}]$$
 (3A)

$$B_{j} = [\delta j] \{ \phi_{j}' - \phi_{j-1}' \} + \delta \phi_{j-1} - [\psi_{j}' - \psi_{j-1}']$$
 (4A)

$$j = k - i + 1 \tag{5A}$$

and

$$\Phi_{i} = 2(i\delta)^{1/2} \tag{6A}$$

$$\psi_{i} = (2/3)(i\delta)^{3/2} \tag{7A}$$

$$\phi_{i}^{'} = \pi^{1/2} (k/a)^{-1/2} \text{ erf } [(k/a)i\delta]^{1/2}$$
 (8A)

$$\psi_{i}^{i} = \frac{\pi^{1/2}}{2} (k/a)^{-3/2} \operatorname{erf}[(k/a)i\delta]^{1/2} - (i\delta)^{1/2} (k/a)^{-1}$$

$$\exp \left[-(k/a)i\delta\right]$$
 (9A)

where

$$\gamma \beta = \exp \left(\frac{nF}{RT}\right) \left(E_i - E^0\right) \tag{11A}$$

$$\gamma\beta\theta = \exp \left(\frac{nF}{RT}\right)\left(E_{i} - E^{0} - E_{s}\right)$$
 (12A)

In the above equations "erf" represents the error function (16) and  $\underline{\mathbf{k}}/\underline{\mathbf{a}}$  is the kinetic parameter (see text).

#### APPENDIX B

# Computer Program

Numerical calculations were performed on a Control Data 3600 digital computer. FORTRAN language was used in the program. To increase versatility of the program wave forms for cyclic voltammetry and potential step-linear scan technique were included. The appropriate wave form is selected through the CONTROL data card (0.0 for cyclic voltammetry and 1.0 for potential step-linear scan). GTLN defines the initial potential, THETA is the step potential, DEL is the width of the integration interval in at units, SQUIG is the number of equations solved to  $a\lambda$  , SSCANS is the number of single scans, LIMIT is the total number of equations to be solved, and PSI is k/a (the kinetic parameter). NTOT is the number of runs for any or all different values of GTLN, THETA, DEL, SQUIG, SSCANS or LIMIT, and NRUN is the number of different kinetic parameters for a given set of the above variables. The output consists of statements of input parameters and five columns of calculated data that are labled CHI(N), CHI(N)-IT, (E-EO)\*N, CZ/CO\*, and AT. These columns contain values of  $\chi(at)$ ,  $\chi(at)$  for the extension of the current-time curve,  $(\underline{E}-\underline{E}^0)$  x  $\underline{n}$ ,  $C_z/C_0^*$  , and at respectively.

```
PROGRAM REVSUC
      DIMENSION SFN (1000), PHI1 (1000), PHI2 (1000), PSI1 (1000),
     1PSI2(1000),Z(1000), CHI(1000),X(1000),SFIT(1000),
     2x1(1000),CHIIT(1000),Z1(1000)
      READ 407, IM, ID, IY
  407 FORMAT (312)
      READ 404, NTOT
    3 READ 404, NRUN
  404 FORMAT (12)
C GTLN IS INITIAL POT--THETA IS STEP POT
C CONTROL = 0 FOR CYCLIC--CONTROL = 1 FOR STEP
      READ 405, GTLN, THETA, DEL, SOUIG, SSCANS, LIMIT
  405 FORMAT (5F10,0,110)
      READ 403, CONTROL
  403 FORMAT (F10.0)
      D = DEL
      IF (CONTROL) 21, 21, 22
   21 CONTINUE
      S=0.
      P = S + 1.
      Q=1.
      I=1
   31 SFN(I)=EXPF(S*DEL*SQUIG-DEL*Q)
      SFIT(I) = SFN(I)
      Q=Q+1.
      I=I+1
      IF(Q-P*SQUIG)31,31,36
   36 S = S + 1.
      P = S + 1.
      IF(P-SSCANS)51,51,50
   51 SFN(I)=EXPF(-P*DEL*SQUIG+DEL*Q)
      SFIT(I) = EXPF(-D*Q)
      Q=Q+1
      I=I+1
      IF(Q-P*SQUIG)51,51,61
   61 S = S + 1.
      P = S + 1.
      IF(P-SSCANS)31,31,50
   22 CONTINUE
      I = 1
   30 \text{ SFN(I)} = \text{EXPF(-THETA)}
      SFIT(I) = SFN(I)
      I = I+1
      QPR = I
      IF(QPR - SQUIG)30,30,35
   35 \text{ XYZ} = \text{LIMIT}
      IF(XYZ - SQUIG)50,50,40
   40 Q = SQUIG + 1
   45 SFN(I) = EXPF(-THETA + D*(Q - SQUIG))
      SFIT(I) = EXPF(-THETA)
      Q = Q + 1.
      I = I+1
      IF(-THETA + D*(Q-SQUIG)) 45,45,50
```

```
50 CONTINUE
C PSI IS K/A
    1 READ 406, PSI
  406 FORMAT(F10.0)
      E = PSI
      SQR = SQRTF(3,14159265/E)
      DO55 N = 1,LIMIT
      Q = N
      PHI1(N) = 2.*SQRTF(Q*D)
      PSI1(N) = \{1, /3, \} *Q*D*PHI1(N)
      PHI2(N) = SQR*PROB(SQRTF(E*Q*D))
      PS12(N) = .5*(PH12(N) - (EXPF(-E*Q*D))*PH11(N))/E
   55 CONTINUE
      GT = EXPF(GTLN)
      A1 = D*PHI1(1) - PSI1(1)
      A2 = D*PHI2(1) - PSI2(1)
      PRINT 200
  200 FORMAT(1H1)
      PRINT 300
  300 FORMAT (50x, 21 HREVERSIBLE SUCCEEDING //)
      IF (CONTROL) 550, 550, 551
  550 PRINT 552
  552 FORMAT (55x, 11HCYCLIC SCAN////////)
      GO TO 554
  551 PRINT 553
  553 FORMAT (56x, 9HSTEP-SCAN////////)
  554 PRINT 301, im, ID, IY
                            12,1H/12,1H/12///)
  301 FORMAT (100x, 7HDATE
      IF (CONTROL) 555,555,556
  555 \text{ SP} = (GTLN - SQUIG*D)*25.68857
      PRINT 557, GTLN
  557 FORMAT (1x, 10HLN(THETA) = F6.3/)
      PRINT 558, SP
  558 FORMAT (1x, 14HSWITCHING POT= F8.3, 12H MV. PAST EO/)
      PRINT 590, SSCANS
  590 FORMAT (24H NUMBER OF SINGLE SCANS= F6.0///)
      GO TO 561
  556 \text{ SP} = 25.68857*(GTLN - THETA)
      DS = D*SQUIG
      PRINT 559, SP
  559 FORMAT (1x, 16HPOTENTIAL STEP = F8.3, 12H MV. PAST EO/)
      PRINT 560, DS
  560 FORMAT (1x, 22HDURATION OF POT-STEP = F8.3, 9H AT UNITS///)
  561 PRINT 562, DEL, SQUIG, LIMIT, PSI
  562 FORMAT (1x, 7HDELTA = F8.4, 2x, 8HLAMBDA = F6.1, 2x,
     17HLIMIT = $15,2x,5HK/A = F10.5///)
      PRINT 563
  563 FORMAT (25x, 6hChi(n), 7x, 9hChi(n)-ir, 4x, 8h(e-e0)*n, 6x,
     16HCZ/CO*, 10X, 2HAT///
      DO 100 N = 1, LIMIT
      Z(N) = A1 + GT*SFN(N)*A2
      Z1(N) = A1 + GT*SFIT(N)*A2
```

```
B1 = 0.0
   B2 = 0.
   C1 = 0.0
   C2 = 0.
   Q = N
   L = N - 1
   DO 101 I = 1,L
   M = N-I
   R = I
   S = Q - R + 1,
              + X(I)*(D*S (PHI1(M+1) - PHI1(M)) + D*PHI1(M) -
   B1 = B1
   1(PSI1(M+1) - PSI1(M))
                      *(D*S*(PHI1(M+1) - PHI1(M)) + D*PHI1(M) -
   B2 = B2+X1(I)
   1(PSI1(M+1) - PSI1(M)))
               + x(1)*(D*S*(PHI2(M+1) - PHI2(M)) + D*PHI2(M) -
   C1 = C1
   1(PSI2(M+1) - PSI2(M))
                      *(D*S*(PHI2(M+1) - PHI2(M)) + D*PHI2(M) -
   C2 = C2 + X1(I)
   1(PSI2(M+1) - PSI2(M)))
101 CONTINUE
   X(N) = (1,77245 - B1 - GT*SFN(N)*C1
                                            )/z(n)
   X1(N) = (1,77245 - B2 - GT*SFIT(N)*C2)/Z1(N)
   CHI(N) = D*X(N) + CHI(N-1)
    CHIIT(N) = D*X1(N) + CHIIT(N-1)
         = 25,68857*(GTLN+LOGF(SFN(N)))
    POT
   B1 = B1 + X(N)*A1
   C1 = C1 + X(N)*A2
   C1 = B1 - C1
   AT = D*Q
   PRINT 66, CHI(N), CHIIT(N), POT, C1, AT
 66 FORMAT (20x, 2F14.8,F12.4, F14.8, F12.3)
100 CONTINUE
   NRUN = NRUN -1
    IF (NRUN)2,2,1
 2 \text{ NTOT} = \text{NTOT} -1
    IF(NTOT)74,74,3
 74 CONTINUE
    PRINT 200
   END
    FUNCTION PROB(A)
    C1 = 0.0705230784
    C2 = 0.0422820123
    C3 = 0.0092705272
    C4 = 0.0001520143
    C5 = 0.0002765672
    C6 = 0.0000430638
   OPROB = 1, - (1, + A*(C1 + A*(C2 + A*(C3 + A*(C4 + A*(C5
   1+ A*C6)))))**(-16.)
    RETURN
    END
```